Journal of Non-Newtonian Fluid Mechanics 298 (2021) 104672

Contents lists available at ScienceDirect

Journal of Non-Newtonian Fluid Mechanics

journal homepage: www.elsevier.com/locate/jnnfm

The Oldroyd-B fluid in elastic instabilities, turbulence and particle suspensions

Eric S.G. Shaqfeh [a,*,1], Bamin Khomami [b,1]

[a] Departments of Chemical and Mechanical Engineering, Stanford University, Stanford, CA 94305, United States of America
[b] Department of Chemical and Biomolecular Engineering, University of Tennessee, Knoxville, TN, United States of America

ARTICLE INFO

Keywords:
Polymer solutions
Hookean dumbbell model
Elastic instabilities
Turbulent drag reduction
Particle suspensions

ABSTRACT

The Oldroyd-B fluid has become the starting point for almost all complex flow calculations and analysis involving the behavior of dilute polymer solutions. The reasons for this are clear: based on the kinetic theory of high molecular weight "phantom" chains near equilibrium, the resulting model, in its simplest form, produces a single mode description of the solution constitutive equation in terms of a single symmetric dyad order parameter. The physical connection to the individual chains is therefore unambiguous through the end-to-end configuration tensor. The flow of the fluid resulting from the mathematical solution of the constitutive equation coupled to Cauchy's equation of motion and continuity has been examined for decades and its strengths and weaknesses in predicting the features of non-linear viscometric and non-viscometric polymer solution flows are well known. Moreover, "simple" extensions (e.g. the FENE-P model) can ameliorate the most serious of these shortcomings. For example, the multi-mode Oldroyd-B model can provide quantitative predictions of the linear viscoelasticity of a wide range of polymer solutions. Remarkably, even with all its shortcomings, the Oldroyd-B fluid has been invaluable in predicting at least qualitatively, features as complex as purely elastic instabilities, turbulent drag modification, and even the effective rheology of particles suspended in polymer solutions. While remaining mindful of the model's shortcomings, any student of these diverse fields may find the Oldroyd-B fluid an important starting point.

1. Introduction: Reasons the Oldroyd-B fluid is used as a starting point for understanding complex elastic fluid phenomena

As reviewed repeatedly in this special issue, the Oldroyd-B fluid (also referred to as the "OB fluid") represents a constitutive equation coupled to Cauchy's equation of motion and continuity which originally arose from Oldroyd's seminal 1950 paper [1]. Upon perusing that paper, however, one finds that the derivation is entirely one associated with the classical mechanics of viscoelastic fluid flow. Thus the OB fluid is one of a class of many "Oldroyd fluids"[1], all which are, from the view point of mechanics, equally possible descriptions of a given elastic fluid. One might wonder then why this particular flavor has formed the basis for so many studies of complex flows of elastic fluids — including studies of elastic instabilities, polymer-induced turbulent drag modification, and even particle suspensions in elastic fluids. The answer lies in at least three related facts: (1) it is a model which is relatively simple including a single conformation tensor to define the state of stress in the liquid as a function of only two parameters (the polymer concentration parameter and the Weissenberg or Deborah number); (2) the OB fluid arises from the simplest kinetic theory of solutions of long chain polymers in flow and (3) experimental studies have demonstrated that the model can quantitatively describe the non-linear steady shear rheology of so-called "Boger" fluids [2]. Moreover, the multimode version of the OB fluid can quantitatively describe the linear viscoelasticity of a wide range of polymer solutions, even those which are not strictly "Boger" fluids. We shall discuss these facts in turn to provide a foundation for understanding the physics that the model includes as it relates to polymer solutions.

1.1. Kinetic theory of a polymer chain in solution and the Oldroyd-B model

As mentioned above, it is primarily the physical connection of the Oldroyd-B model to real elastic liquids (i.e polymer solutions) which makes it a model of choice. Thus, it is appropriate to review that connection through its derivation from the kinetic theory of polymer solutions. This derivation can be found in much more detail elsewhere [3] and we provide only a brief review here. A high molecular weight,

* Corresponding author.
E-mail address: esgs@stanford.edu (E.S.G. Shaqfeh).
[1] Both authors contributed equally to this article.

https://doi.org/10.1016/j.jnnfm.2021.104672
Received 16 May 2021; Received in revised form 3 October 2021; Accepted 5 October 2021
Available online 16 October 2021

flexible polymer in a θ solvent is characterized by a nearly Gaussian probability of end-to-end vector as its configuration is, to an excellent approximation, given by a random walk of N_k steps. Thus, Kuhn [4] originally said that for very flexible, *idealized* [5] chains, the gross statistical features were that of a random walk where b_k =step size or Kuhn step size and N_k is the number of Kuhn steps

$$b_k N_k = L = lP$$

where l = length of a monomer (projected along the direction of chain extension), P = number of monomers in the chain, and L is the maximum length of the chain. For a freely jointed random walk (no excluded volume) the distribution function of end to end distance $\psi(\vec{R})$ can be approximated as a Gaussian for $R = |\vec{R}| < b_k N_k$ and in the limit $N_k \to \infty$

$$\psi(\vec{R}) = (\frac{\kappa}{\sqrt{\pi}})^3 \exp(-\kappa^2 R^2) \tag{1}$$

$$\kappa^2 = 3/2N_k b_k^2, \quad < R^2 >= N_k b_k^2, \tag{2}$$

and the angle brackets refer to the average over $\psi(\vec{R})$. Note that the ratio $\frac{<R^2>}{Pl^2} = C_\infty$ (where **l** is the unprojected monomer length) is called the *characteristic ratio* and has been tabulated for a given chain. Now the number of internal configurations available at a given stretch, $\vec{R}$ is proportional to the probability $\psi(\vec{R})$, i.e. $\Omega = c\psi(\vec{R})$; $c = constant$, and from statistical mechanics the entropy, S is given by $S = k \log \Omega$. Thus, the entropic contribution to the free energy W is

$$W = -TS = -kT \log \Omega$$

It follows then that the work necessary to stretch the chain from R_i to $R_i + dR_i$ is (using indicial notation) $\frac{\partial W}{\partial R_k} dR_k$ from "the principle of virtual work" . Thus, the entropic force acting on the ends of the chain for a given stretch $\vec{R}$ is $\mathcal{F}_m = -F_m$; where F_m is the force one needs exert to stretch the chain. It follows that

$$F_m dR_m = \frac{\partial W}{\partial R_k} dR_k \quad and \quad F_i = -kT \frac{\partial(\log \psi)}{\partial R_i} \tag{3}$$

This argument is therefore equivalent to the thermodynamic argument of Einstein namely that there is an effective force proportional to the gradient of the *log* of the probability density. Taking the derivatives then

$$\mathcal{F}_i = -F_i = -2kT\kappa^2 R_i = -\frac{3kT}{N_k b_k^2} R_i = -H R_i \tag{4}$$

Thus the entropic restoring force is linear in the end to end distance with spring constant H and this is often referred to as the **"Hookean spring" model**. It follows then that in a flow which scales on lengths larger than the characteristic polymer scale (e.g. radius of gyration) the entire center of mass and configuration of the chain can be specified approximately by the equations for the rate of change of the center of mass $\vec{x}$ and the rate of change of $\vec{R}$ as:

$$\frac{dx_i}{dt} = u_i(x_i) - \frac{kT}{2\zeta} \frac{\partial}{\partial x_i} \log \Psi \tag{5}$$

$$\frac{dR_i}{dt} = R_j \mathcal{L}_{ij} - \frac{4kT\kappa^2}{\zeta} R_i - \frac{2kT}{\zeta} \frac{\partial}{\partial R_i} \log \Psi, \tag{6}$$

where we have assumed that the drag coefficient ζ is a constant and where $\Psi(\vec{x}, \vec{R}, t)$ is the distribution function for both center of mass and conformation. In the expressions above $u_i(x_i)$ is the velocity of the fluid and $\mathcal{L}_{ij} = \frac{\partial u_i}{\partial x_j}$ is the transpose of the velocity gradient tensor. **The drag coefficient ζ is equivalent to the drag on "half" the chain, and with this specification, we have the so-called "linear dumbbell model"**. With $\xi = \frac{4kT\kappa^2}{\zeta}$, $\mathcal{D} = \frac{kT}{2\zeta}$, and $D = \frac{2kT}{\zeta}$ the Fokker–Planck equation for Ψ becomes:

$$\frac{\partial \Psi}{\partial t} + \frac{\partial}{\partial x_i}[u_i(\vec{x})\Psi] - \mathcal{D}\frac{\partial^2}{\partial x_k \partial x_k}[\Psi] + \frac{\partial}{\partial R_i}(\mathcal{L}_{ij} R_j \Psi) - \frac{\partial}{\partial R_i}[\xi R_i \Psi] - D\frac{\partial^2}{\partial R_k \partial R_k}(\Psi) = 0$$

Simplifications are often made at this point including:

- The center of mass Péclet number, $Pe \gg 1$ so that Brownian motion of the center of mass can be neglected. Note the Schmidt number of a high molecular weight polymers is typically enormous.
- The center of mass probability is homogeneous and equal to n_p, the number density of polymers. Thus:

  $\Psi = n_p \psi(\vec{R}, t; \vec{x})$

  where the normalization of the configuration probability ψ is $\int \psi d\vec{R} = 1$.

With these simplifications we have:

$$\frac{D\psi}{Dt} + \frac{\partial}{\partial R_i}[\mathcal{L}_{ij} R_j \psi] - \frac{\partial}{\partial R_i}[\xi R_i \psi] - D\frac{\partial^2}{\partial R_k \partial R_k}[\psi] = 0, \tag{7}$$

The extra stress in these polymer solutions can now be determined approximately using this linear force model via the Kramers–Kirkwood relationship [6] as:

$$\sigma_{ij}^P = n_P kT \left[2\kappa^2 < R_j R_i > -\delta_{ij}\right] \tag{8}$$

and thus is proportional to an order parameter $\left[2\kappa^2 < R_j R_i > -\delta_{ij}\right]$. Note that the Kramers–Kirkwood relationship and the resulting stress is entirely equivalent to the "stresslet" derivation of the extra stress from suspension mechanics [7] if one accepts the dumbbell model as two equal and opposite point forces separated by a spring, or equivalently, a force dipole. Note since the stress depends only on the second moment of the conformation distribution, we can multiply the Fokker–Planck equation by $R_i R_j$ and integrate over conformation space using the divergence theorem to obtain:

$$\frac{D < R_i R_j >}{Dt} - \mathcal{L}_{il} < R_l R_j > -\mathcal{L}_{jl} < R_l R_i > + \frac{1}{\lambda} < R_i R_j >= 2D\delta_{ij}, \tag{9}$$

or alternatively,

$$\lambda \left[\frac{D < R_i R_j >}{Dt} - \mathcal{L}_{il} < R_l R_j > -\mathcal{L}_{jl} < R_l R_i >\right] + < R_i R_j >= \frac{N_k b_k^2}{3}\delta_{ij}, \tag{10}$$

where $\lambda = \frac{1}{2\xi}$. It is worth noting that λ, which is now the relaxation time in the model, is proportional to the time it takes for the chain to diffuse a distance $\sqrt{N_k b_k^2}$, i.e. a measure of its equilibrium coil radius. Finally, using the relation between the second moment and the stress, we can write a direct equation for σ_{ij}^P

$$\lambda[\frac{D\sigma_{ij}^P}{Dt} - \mathcal{L}_{ik}\sigma_{jk}^P - \mathcal{L}_{jk}\sigma_{ik}^P] + \sigma_{ij}^P = \lambda \overset{\nabla}{\sigma}_{ij}^P + \sigma_{ij}^P = 2\eta_p E_{ij}; \quad \eta_p = n_p kT\lambda, \tag{11}$$

where η_p is termed the "polymer viscosity", $E_{ij} = \frac{1}{2}\left[\mathcal{L}_{ij} + \mathcal{L}_{ji}\right]$ is the rate of strain tensor, and $\overset{\nabla}{[\cdot]}$ is the upper convected derivative. Eqs. (10) and (11) are the *Maxwell model* for the conformation and polymer stress respectively, with the elasticity of the chain being defined by a single linear relaxation. Writing the total stress now as:

$$\sigma_{ij} = -P\delta_{ij} + 2\eta_s E_{ij} + \sigma_{ij}^P \tag{12}$$

(i.e. adding a Newtonian contribution to the deviatoric stress characterized by a "solvent" viscosity, η_s,) and combining with Cauchy's equation of motion and continuity, we have the (incompressible) Oldroyd-B fluid. This is remarkable, because this derivation is seemingly very different than that imagined by Oldroyd some 70 years ago. Thus, as mentioned above, the Oldroyd-B fluid becomes the simplest model for high molecular weight polymer solutions and its predictions can, through the elements of this derivation, be related to polymer conformation change. The successes and limitations of the model can therefore be given a direct physical interpretation and in the present day – especially, since single molecule studies of high molecular weight polymers have been accomplished with unprecedented precision (e.g. [8]) in a variety of flows – the limitations have become common scientific knowledge. We discuss the predictions of the Oldroyd-B model in simple flows below.

1.2. The Oldroyd-B model in simple shear flow

Thus as is typically done, we will non-dimensionalize the Oldroyd-B fluid equations in simple shear flow in the following way (with $\eta_T = \eta_S + \eta_P$); $\bar{\sigma}^P_{ij} \cdot \eta_P \dot{\gamma} = \sigma^P_{ij}$; $\bar{\sigma}_{ij} \cdot \eta_T \dot{\gamma} = \sigma_{ij}$ and where $\tau = \dot{\gamma} t$ – thus we use the inverse shear rate $\dot{\gamma}^{-1}$ as a time scale. It follows that

$$\bar{\sigma}_{ij} = -\bar{P}\delta_{ij} + 2\beta \bar{E}_{ij} + (1-\beta)\bar{\sigma}^P_{ij}$$

where $\frac{\eta_S}{\eta_T} = \beta$ is a dimensionless polymer concentration parameter. (If, $\beta = 0$, all stress is polymeric and the fluid is usually referred to as the *Maxwell fluid*). The dimensionless constitutive equation becomes:

$$Wi[\frac{D\bar{\sigma}^P_{ij}}{D\tau} - \bar{\mathcal{L}}_{il}\bar{\sigma}^P_{jl} - \bar{\mathcal{L}}_{jl}\bar{\sigma}^P_{il}] + \bar{\sigma}^P_{ij} = 2\bar{E}_{ij} \tag{13}$$

where $Wi = \lambda\dot{\gamma}$ is the *Weissenberg number*. From the definition of simple shear flow then $u_i = \dot{\gamma} x_2 \delta_{i1}$, $\mathcal{L}_{ij} = \dot{\gamma}\delta_{i1}\delta_{j2}$, $E_{ij} = \frac{\dot{\gamma}}{2}[\delta_{i1}\delta_{j2} + \delta_{j1}\delta_{i2}]$, $\bar{\mathcal{L}}_{ij} = \delta_{i1}\delta_{j2}$, and $\bar{E}_{ij} = \frac{1}{2}(\delta_{i1}\delta_{j2} + \delta_{j1}\delta_{i2})$. Simple physical arguments allow one to conclude that the only components of the stress $\bar{\sigma}^P_{ij}$ that could be nonzero are $\bar{\sigma}^P_{11}, \bar{\sigma}^P_{12} = \bar{\sigma}^P_{21}$, and $\bar{\sigma}^P_{22}$. Writing then the steady stress equations:

$$Wi\{-\delta_{i1}\bar{\sigma}^P_{j2} - \delta_{j1}\bar{\sigma}^P_{i2}\} + \bar{\sigma}^P_{ij} = (\delta_{i1}\delta_{j2} + \delta_{j1}\delta_{i2})$$

It follows solving term by term that:

$$\bar{\sigma}^P_{11} = 2Wi;\ \bar{\sigma}^P_{12} = 1;\ \bar{\sigma}^P_{22} = 0,$$

or, in dimensional terms

$$\sigma^P_{11} = 2\lambda\eta_P\dot{\gamma}^2;\quad \sigma^P_{12} = \eta_P\dot{\gamma};\quad \sigma^P_{22} = 0 \tag{14}$$

for all shear rates. This naturally leads us to the 3 material functions for shear flow (following from the 3 unique non-zero components of the stress in shear), $\frac{\sigma_{12}}{\dot{\gamma}} = \eta$ (the shear viscosity), $\frac{\sigma_{11}-\sigma_{22}}{\dot{\gamma}^2} = \Psi_1$ (the primary normal stress coefficient) and $\frac{\sigma_{22}-\sigma_{33}}{\dot{\gamma}^2} = \Psi_2$ (the second normal stress coefficient). Thus for the Oldroyd-B fluid

$$\eta = \eta_S + \eta_P = \eta_T,\quad \Psi_1 = 2\eta_P\lambda,\quad \Psi_2 = 0. \tag{15}$$

and all shear material parameters are constants. At this point, we mention the *multi-mode* Oldroyd-B, which is more precisely, a multi-mode Maxwell model with the addition of a solvent viscosity. Thus, each polymer stress mode n, $\sigma^{P(n)}_{ij}$, satisfies its own Maxwell equation, viz.

$$\lambda^{(n)}[\frac{D\sigma^{P(n)}_{ij}}{Dt} - \mathcal{L}_{ik}\sigma^{P(n)}_{jk} - \mathcal{L}_{jk}\sigma^{P(n)}_{ik}] + \sigma^{P(n)}_{ij}$$
$$= \lambda\ \overset{\nabla}{\sigma}{}^{P(n)}_{ij} + \sigma^{P(n)}_{ij} = 2\eta^{(n)}_p E_{ij};\quad \eta^{(n)}_p = n_p kT\lambda^{(n)}, \tag{16}$$

with the appropriate series of material parameters, $\eta^{(n)}_P$ and $\lambda^{(n)}$ and with the total polymer stress a linear combination of the individual stress components, viz. $\sigma^P_{ij} = \sum_{n=1}^N \sigma^{P(n)}_{ij}$. Thus in simple shear for the multi-mode Oldroyd-B we have:

$$\sigma^P_{11} = \sum_{n=1}^N 2\lambda^{(n)}\eta^{(n)}_P\dot{\gamma}^2;\quad \sigma^P_{12} = \sum_{n=1}^N \eta^{(n)}_P\dot{\gamma};\quad \sigma^P_{22} = 0,\qquad \eta = \eta_S + \sum_{n=1}^N \eta^{(n)}_P,$$
$$\Psi_1 = \sum_{n=1}^N 2\lambda^{(n)}\eta^{(n)}_P. \tag{17}$$

1.3. The Oldroyd-B model in linear viscoelasticity

From the above results it is easy to develop the expressions for the Oldroyd-B model in "weak" linear oscillatory shear flow – i.e. linear viscoelasticity. Thus with $u_i = \dot{\gamma}\delta_{i1}x_2\exp i\omega t$ and defining $\tau = t/\lambda$ and $\bar{\omega} = \lambda\omega$, we have in the asymptotic limit [9,10] as $Wi \to 0$ but $\bar{\omega} \sim O(1)$ and $\bar{\sigma}^P_{ij} \sim O(1)$,

$$\frac{\partial\bar{\sigma}^P_{ij}}{\partial\tau} + \bar{\sigma}^P_{ij} = 2\bar{E}_{ij};\quad \bar{E}_{ij} = \frac{1}{2}(\delta_{i1}\delta_{j2} + \delta_{i2}\delta_{j2})\exp i\bar{\omega}\tau$$

We mention that the asymptotic limit $Wi \to 0$ is equivalent to the "small amplitude" oscillatory shear limit, since for a shear strain γ in a device of a finite shear gap, the appropriate Weissenberg number can alternatively be written $Wi = \gamma\omega\lambda$ (since $\dot{\gamma} \propto \gamma\omega$). So γ (which is proportional to the amplitude of oscillation) must be vanishingly small at any $\bar{\omega}$ if the nonlinearities in the constitutive equation are to be neglected. Solving for the only non-zero component of the stress, yields the complex shear stress:

$$\bar{\sigma}^P_{12} = \bar{\sigma}^P_{21} = \frac{1}{1+i\bar{\omega}}\exp i\bar{\omega}\tau = \frac{1-i\bar{\omega}}{1+\bar{\omega}^2}\exp i\bar{\omega}\tau \tag{18}$$

From the definition of the complex viscosity, $\bar{\eta}^* = \frac{\eta^*}{\eta_T} = \frac{\eta' - i\eta''}{\eta_T}$, we have for the real and imaginary parts:

$$\eta' = \eta_S + \frac{\eta_P}{1+\bar{\omega}^2},\quad \eta'' = \frac{\eta_P\bar{\omega}}{1+\bar{\omega}^2} \tag{19}$$

or alternatively in terms of the moduli

$$G' = n_p kT\frac{\bar{\omega}^2}{1+\bar{\omega}^2};\quad G'' = \eta_S\omega + n_p kT\frac{\bar{\omega}}{1+\bar{\omega}^2} \tag{20}$$

The multi-mode version of the moduli and complex viscosity follows immediately as

$$\eta' = \eta_S + \sum_{n=1}^N \frac{\eta^{(n)}_P}{1+\bar{\omega}^{(n)2}},\quad \eta'' = \sum_{n=1}^N \frac{\eta^{(n)}_P\bar{\omega}^{(n)}}{1+\bar{\omega}^{(n)2}} \tag{21}$$

$$G' = n_p kT\sum_{n=1}^N \frac{\bar{\omega}^{(n)2}}{1+\bar{\omega}^{(n)2}};\quad G'' = \eta_S\omega + n_p kT\sum_{n=1}^N \frac{\bar{\omega}^{(n)}}{1+\bar{\omega}^{(n)2}} \tag{22}$$

where $\bar{\omega}^{(n)} = \lambda^{(n)}\omega$. The advantage for the multi-mode model in linear viscoelasticity is clear as shown in the comparisons to data below. Thus, if the correct spectrum is chosen, the multi-mode Oldroyd B can reproduce either the Rouse [11] or Zimm [12] results from linear viscoelasticity and therefore can usually reproduce the high frequency linear viscoelastic behavior of polymer solutions somewhat faithfully.

1.4. Comparison of Oldroyd-B predictions in shear to "Boger" fluid rheology

For the reasons discussed in Section 1.1, the Oldroyd-B model is typically used as a model for dilute polymer solutions. Since it is well known that the material parameters predicted by the model are not functions of the shear rate, it is, more precisely, used as a model for so-called "Boger fluid" rheology. Boger fluids are a class of polymer solutions originally developed by David Boger [2,13], where a relatively dilute solution of high molecular weight polymer is dissolved in a very viscous, Newtonian solvent (e.g. solvents at least 1000 times more viscous than water). Such a mixture has been shown to produce a fluid that is quite elastic (i.e. relaxation times measured in seconds) and whose primary normal stress coefficient and shear viscosity are nearly constant over decades of shear rate. The original fluids were water-based and thus a typical mixture would consist of corn syrup, water and high molecular weight polyacrylamide. These are now known as "Type 1", Boger fluids [14] ."Type 2" Boger fluids [14] are based on organic solvents, and typically involve a high molecular weight polymer (e.g. 10^6 gg/mol polyisobutylene) dissolved in an oligomeric solvent of the same or similar molecular structure with a small molecule, relatively volatile solvent in the mixture to aid the solvation of the high molecular weight species.

An example of Boger Fluid shear rheology [13] and comparison to the Oldroyd-B model is show in Figs. 1a and 1b. The Boger fluid consists of a high molecular weight polyisobutylene [(PIB) average $M_w \approx 4.2\times10^6$ from Sigma-Aldrich] dissolved in kerosene and mixed with low molecular weight polybutene [(PB) Indopol H-25 from Ineos

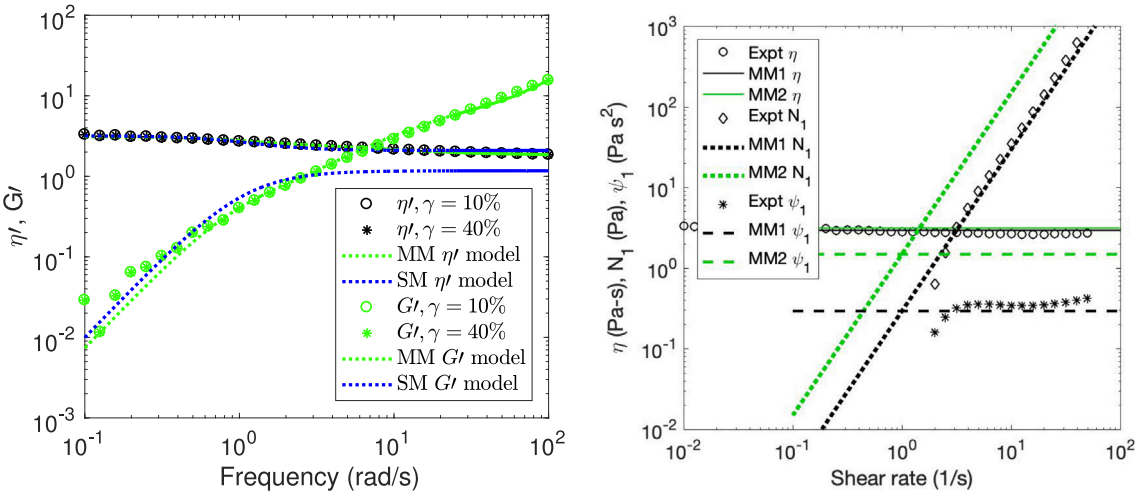

Fig. 1. Single mode and multi-mode fit of Oldroyd-B Model to Boger fluid shear data. (a) LEFT — Linear viscoelastic functions η' and G' with the multimode (MM) and single mode (SM) model predictions. The MM model includes a four mode fit plus a fit to the solvent viscosity. Data is taken at strains of 0.1 and 0.4. (b) RIGHT — Nonlinear material parameters for the same Boger fluid with the predictions of the Oldroyd-B model. "MM2" refers to the multi-mode fit corresponding to the linear viscoelastic data in (a). "MM1" is a new fit only to the nonlinear data.
Source: Modified from [15].

Oligomers Technology]. Thus this is a Type 2 Boger fluid. The solution of PIB in kerosene is made first by dissolving small pieces of PIB (3.4 wt%) in kerosene (96.6 wt%). The PB is then added for a final fluid composition of 92.93 wt% of PB, 6.83 wt% of kerosene, and 0.24 wt% of PIB. This fluid is similar to the benchmark Boger M1 fluid [16] (although the PIB is of somewhat higher MW) where the M1 fluid was used to examine the extensional viscosity of polymer solutions with typical filament stretching data such as that in Fig. 2b below.

The multi-mode model in Fig. 1a is a four mode fit which gives a longest relaxation time of $1s$. The single mode fit gives $0.926s$ to the linear viscoelastic data. Examination of these figures allows one to make three quick conclusions: (a) The multimode fit including four modes is quantitative for the linear viscoelasticity data over three decades in frequency while the single mode model badly underpredicts G' at high frequencies, (2) the same multi-mode Oldroyd B model over-predicts the primary normal stress coefficient but can be made quantitative by fitting just the nonlinear viscoelastic data (thus reducing the longest relaxation time to 0.74 s), and (3) For these Boger fluids the material parameters Ψ_1 and η are weak functions of shear with the latter showing a clear shear thinning that is not captured by the Oldroyd-B model. At least two important physical reasons for the shear thinning are now clear from an abundant literature on the subject: both finite extensibility of the polymer chain as well as intra-chain hydrodynamic interactions (or equivalently a drag coefficient that depends on configuration) both make the polymer contribution to the viscosity a function of shear rate in real polymer solutions at values of $Wi \geq 1$ [8,17]. In the simplest case of finite chain extensibility, it is well known from visualizations of DNA (for example) that as the chain stretches in the flow direction in shear at a point of stretch even below 50% of its maximum extension, the chain will cease to stretch and instead rotate its orientation downward toward the flow axis, thus creating less overall extra dissipation resulting in a "thinning" of the viscosity [8]. Thus in general the Oldroyd-B model is known to overpredict the streamwise polymer stretch in flow at values of $Wi \approx O(1)$ and this is also consistent with the reduction in the apparent relaxation time as determined from the normal stress fits recalling that $\sigma_{11}^P = n_p kT\left[2\kappa^2 < R_1 R_1 > -1\right]$. Nevertheless, it is apparent that the linear and nonlinear shear rheology for this class of fluids is at least qualitatively predicted by the Oldroyd-B model, and, along with its clear physical interpretation from kinetic theory, these are among the strongest reasons for it to be employed at least as a first step.

1.5. Oldroyd-B model in extensional flow and associated FENE models

Consider a uniaxial extensional flow characterized by the dimensional rate of strain tensor,

$$E_{ij} = \dot{\epsilon}\begin{Bmatrix} 1 & 0 & 0 \\ 0 & -1/2 & 0 \\ 0 & 0 & -1/2 \end{Bmatrix}$$

where $\dot{\epsilon}$ is the rate of strain along the line of principal strain, here defined as "1". If we make time and $\mathcal{L}_{ij}$ dimensionless with $\dot{\epsilon}$, and define the *Deborah number* as $De = \dot{\epsilon}\lambda$, the polymer stress within the steady Oldroyd B model becomes:

$$\left.\begin{array}{l} De(-2\bar{\sigma}_{11}^P) + \bar{\sigma}_{11}^P = 2 \\ De(\bar{\sigma}_{22}^P) + \bar{\sigma}_{22}^P = 1 \\ \bar{\sigma}_{22}^P = \bar{\sigma}_{33}^P \end{array}\right\} \begin{array}{l} \bar{\sigma}_{11}^P = \frac{2}{1-2De} \\ \bar{\sigma}_{22}^P = \bar{\sigma}_{33}^P = \frac{1}{1+De} \end{array} \quad (23)$$

Clearly at the critical point $De = 1/2$ we have an unphysical prediction of a stress singularity and this behavior is intrinsic to the OB fluid. This stress singularity manifests itself as a singularity in the Trouton ratio, viz.

$$T_r = \frac{\eta_{ext}}{3\eta_T} = \frac{\sigma_{11} - \frac{1}{2}(\sigma_{22} + \sigma_{33})}{3\eta_T \dot{\epsilon}}$$
$$T_r = \beta + (1-\beta)\left\{\frac{2}{1-2De} - \frac{1}{1+De}\right\} \quad (24)$$

Note that the multi-mode version of the Oldroyd-B does not relieve the singularity as it is governed by the Deborah number based on the longest relaxation time. At or near the point $De \approx 1/2$, it is now well known, that a real, single polymer molecule undergoes a coil–stretch transition that is actually very complex in its dynamics [18,19]. Ultimately (in what might be a very long period of time relative to its relaxation time) the molecule stretches to a large fraction of its maximum extensibility.

It is easy to show that the aforementioned singularity is a result of examining the steady equations, since if one alternatively examines the time dependent (i.e. finite strain) dynamics of the Oldroyd-B model, we have in dimensional form for the conformation tensor component $< R_1^2 >$:

$$\frac{d < R_1^2 >}{dt} - 2\dot{\epsilon} < R_1^2 > + \frac{1}{\lambda} < R_1^2 > = 2D$$

and we can solve to show:

$$< R_1^2 >= \left[< R_1^2 > (0) - \frac{2D}{1/\lambda - 2\dot{\epsilon}}\right] \exp(2\dot{\epsilon} - 1/\lambda)t + \frac{2D}{1/\lambda - 2\dot{\epsilon}} \tag{25}$$

Clearly for $2\dot{\epsilon} - 1/\lambda > 0$, or $(De > 1/2)$ we get exponential growth of the configuration and hence the stress. This growth is only bound by the *Hencky* strain $\dot{\epsilon}t$. Exponential growth to an unbound polymer stretch is clearly unphysical (see discussion below regarding experiments and comparison to fine-grained models), and thus a failure of the physical model upon which the Oldroyd B is based. It is associated with the fact that the principle of virtual work argument was originally conceived for small departures from equilibrium, thus producing a linear restoring force that can be overwhelmed by a linearly increasing rate of chain stretch by the flow. Thus, there is a simple "fix" that is used almost universally in flows where there are points of local extensional flow. Returning to the original linear restoring force which is the physical foundation for the kinetic theory which yields the Oldroyd-B fluid, one simply allows the force to "stiffen" as the chain becomes more stretched, viz.

$$\mathcal{F}_i = -\frac{3kT}{N_k b_k^2} f(R) R_i$$

where $f(R)$ (with $R = |R_i|$) is a stiffening function representing the increased work necessary to deform the chain as it becomes increasingly stretched (due to the reduction in the entropic states available as the chain is stretched to a significant fraction of its maximum extensibility). Statistical mechanics does give us models for $f(R)$ and, for example, if $L = N_k b_k$ is the maximum extension of the chain, then, for freely jointed chains where all internal modes are allowed to equilibrate [4], $f = [L\mathbb{L}^{-1}(R/L)]/3R$, and $\mathbb{L}^{-1}$ is the inverse Langevin function (ILF) where $\mathbb{L}(x) = \coth(x) - 1/x$. Since the ILF is not easily expressible in terms of simple functions, various approximate forms have been used in the literature, including the Warner spring (or the FENE model) [20] and Cohen's Pade approximate to the ILF, [21] which are respectively

$$f_{FENE} = \frac{1}{1 - (R/L)^2} \qquad f_{ILC-CP} = \frac{1 - (R/\sqrt{3}L)^2}{1 - (R/L)^2}, \tag{26}$$

where ILC refers to the Inverse Langevin Chain. Note that only the latter is asymptotically correct for both large and small deformations [21], although both approximations demonstrate the same strength of singularity (i.e. a pole) as $R/L \to 1$. Chains which are not freely jointed, but demonstrate a finite bending modulus along their backbone, are referred to as worm-like chains (WLC) and one typically, in this instance, employs the worm-like spring model [22]:

$$f_{WLC} = \frac{L}{6R}\left[\frac{1}{(1 - R/L)^2} - 1 + \frac{4R}{L}\right] \tag{27}$$

to describe their stiffening. This model has been shown to be quantitative for DNA chains, for example. All models are finitely extensible and therefore avoid the configurational singularity that is in the Oldroyd B model. However, the average of the first moment of the restoring force (i.e. the stress) now depends on higher moments of the chain conformation and hence a closed form constitutive equation is not immediate without additional approximations, including the common "pre-averaging" approximation [23]:

$$\mathcal{F}_i \approx -\frac{3kT}{N_k b_k^2} f(\tilde{R}) R_i; \quad \tilde{R} = \sqrt{< R^2 >}$$

It is beyond the scope of this article to discuss the large body of literature on the accuracy of this approximation [23,24], but it does yield a simple modified version of the Oldroyd-B since $f(\tilde{R})$, is now a constant as far as averaging over the distribution function ψ. Hence, in the same notation, the equation corresponding to Eq. (10), for the polymer conformation dyad is:

$$\lambda\left[\frac{D < R_i R_j >}{Dt} - \mathcal{L}_{il} < R_l R_j > - \mathcal{L}_{jl} < R_l R_i >\right] + f(\tilde{R}) < R_i R_j >= \frac{N_k b_k^2}{3}\delta_{ij} \tag{28}$$

with the corresponding expression for the polymer stress as:

$$\sigma_{ij}^P = n_P kT\left[2\kappa^2 f(\tilde{R}) < R_j R_i > -\delta_{ij}\right] = n_P kT\left[\frac{3}{N_k b_k^2} f(\tilde{R}) < R_j R_i > -\delta_{ij}\right]$$
$$= -\frac{3\eta_P}{N_k b_k^2}\left[< R_j \overset{\nabla}{R}_i >\right]. \tag{29}$$

If $f = f_{FENE}$ this is referred to as the *FENE-P model*. There are multi-mode versions of this as well, although decisions must be made as to $\tilde{R}$ for each mode since in general the modes in the model before pre-averaging are nonlinearly coupled. The multi-mode version that is in most common use is the so-called *FENE-PM* [25]. It is reasonably straightforward to demonstrate that for the uniaxial extensional flow, the FENE-P model gives at steady state for $De \gg 1$

$$< R_1^2 > \sim N_k^2 b_k^2\{1 - \frac{1}{2De} + \cdots\}, \quad \sigma_{11}^p \approx 6 n_p kT N_k De, \quad Tr \approx \beta + (1-\beta)2N_k$$

Thus indeed the polymer conformation and Trouton ratio are bound for values of De past the coil to stretch transition, and are limited by the maximum extensibility of the chain $L = N_k b_k$.

For comparison to other literature that we will discuss below, it is worthwhile to mention the typical dimensionless form of Eq. (28); viz

$$De\left[\frac{D\overline{< R_i R_j >}}{Dt} - \bar{\mathcal{L}}_{il}\overline{< R_l R_j >} - \bar{\mathcal{L}}_{jl}\overline{< R_l R_i >}\right] + f(\bar{R})\overline{< R_i R_j >} = \delta_{ij} \tag{30}$$

where $\overline{< R_i R_j >} = 3 < R_i R_j > /(N_k b_k^2)$ and $\bar{R} = \sqrt{\overline{< R_i R_j >}}$. With this nondimensionalization the FENE-P function is often written:

$$f_{FENE} = \frac{1}{1 - \bar{R}^2/\mathrm{b}} \tag{31}$$

where $\mathrm{b} = \frac{3L^2}{N_k b_k}$. The polymer stress in terms of the dimensionless second moment is $\sigma_{ij}^P = n_P kT\left[f(\bar{R})\overline{< R_j R_i >} - \delta_{ij}\right]$.

We can also mention at this point the *Giesekus model* [26] for comparison purposes to the Oldroyd-B and FENE-P. This model, suggested by Giesekus [26], is not a modification of the OB Fluid, even though the equations are similar. It is derived by assuming that the drag coefficient on a given chain is affected by surrounding chains and is a tensor depending on local mean field polymer stretch. It therefore is fundamentally, a *non-dilute model* for polymer solutions. The model, with the same non-dimensionalization as above, can be written:

$$De\left[\frac{D\overline{< R_i R_j >}}{Dt} - \bar{\mathcal{L}}_{il}\overline{< R_l R_j >} - \bar{\mathcal{L}}_{jl}\overline{< R_l R_i >}\right]$$
$$+ \overline{< R_i R_j >} - \delta_{ij} + \alpha\left[\overline{< R_i R_j >} - \delta_{ij}\right]^2 = 0, \tag{32}$$

where $a_{ij}a_{jk} = a_{ik}^2$ and $\sigma_{ij}^P = n_P kT\left[\overline{< R_j R_i >} - \delta_{ij}\right]$. Note this model also does not exhibit a stress singularity in extension, but for very different reasons than the FENE-P. In this case the drag coefficient on the chain *decreases* with increasing extension (i.e. represented by the last quadratic term on the left side of Eq. (32)), and hence by this model, the chain is increasingly difficult to stretch in extension. The new parameter α is a dimensionless measure of drag anisotropy and, by inspection, if $\alpha = 0$, we recover the OB fluid (i.e. the polymer stress is again governed by the Maxwell model).

Although, we have introduced the FENE models and the Giesekus model within the context of "fixing" the extensional stress singularity inherent in the Oldroyd B model, we should note that both FENE and Giesekus models demonstrate "shear thinning" of the material

parameters in simple shear. Thus, one can argue that these models also "fix" the comparison of the Oldroyd B to the nonlinear shear data shown in Fig. 1. To be specific, with certain values of the model parameters, the nonlinear shear viscosity and primary normal stress coefficient of polymer solutions can be quantitatively reproduced by the FENE and Giesekus models — and multi-mode versions then reproduce the linear viscoelasticity. This is actually how the parameters $\mathfrak{b}$ and α are often chosen in comparing experiments to numerical simulations. Note that this has the disadvantage of disconnecting these parameters from kinetic theory and making them true "fitting" parameters. For example, the value of $L = N_k b_k$ is fixed by single molecule theory, but the resulting $\mathfrak{b}$ for high molecular weight polymer solutions is much larger than often used in calculations or in "fits" to rheological data.

1.6. Comparison of Oldroyd-B model in extensional flow to fine-grained models and experiments

In Fig. 2a, we show typical comparison of the polymer contribution to the extensional viscosity for the single and multimode Oldroyd-B model as a function of Hencky strain versus a Kuhn step level model of a polymer – i.e. a freely-jointed bead-rod chain of 200 links without hydrodynamic interactions along the backbone. The latter simulation is accomplished via Brownian dynamics [27]. The Oldroyd B model(s) show exponential growth of the viscosity at $De = 10.65$ (which is well above the critical value) for almost all but the smallest values of strain. The comparison demonstrates two points: First, the departure of the Oldroyd-B model from the fine-grained model occurs around $\dot{\epsilon}t \approx 2$ and the Oldroyd-B actually underpredicts the stress for higher strains, until $\dot{\epsilon}t \approx 5$ when the finite extensibility of the chain causes the extensional viscosity to plateau at a high value. The second important conclusion is that multi-modes are necessary to get quantitative agreement with the extensional viscosity even for $\dot{\epsilon}t \leq 2$. In this latter case, the longest relaxation time of the Oldroyd-B model was fixed to that of the bead-rod chain, then the higher modes were that of the equivalent *Rouse* chain [11]. It is clear that at least 5 modes are necessary to obtain quantitative agreement.

In Fig. 2b, we compare FENE models to the extensional stress measured in a high molecular weight polystyrene Boger solution [28]using a filament stretching device. Both single mode and multi-mode FENE models are included. Note that now the model predictions are such that the plateau or steady extensional stress is reached for $\dot{\epsilon}t \approx 6$ and the stress singularity of the Oldroyd-B is indeed relieved. Again, the multi-mode model does a much better job of predicting the stress at small strains. However the prediction of the FENE models is not quantitative at strains in excess of 3. There is now quite a wide literature on the physical aspects of a polymer model necessary to get quantitative agreement with extensional data from the filament stretching device — which as an aside are considered the best such measurements of the extensional properties of polymer solutions. As described in the review by McKinley & Sridhar [29], the FENE-P and FENE-PM models "consistently underpredict the stress growth at intermediate strains and predict a much more rapid transition to the final steady state". Li, Larson, and Sridhar (2000) [30] as well as Saadat & Khomami [31] demonstrated unequivocally that hydrodynamic intra-chain interactions and multi-modes are necessary to attain quantitative agreement with extensional data in Boger fluids. Note that intra-molecular hydrodynamic interactions, introduce, in a coarse-grained sense, *conformation-dependent drag* [27,32,33]. These effects are not present in the OB or FENE-P models. Moreover, we also now know that the conformation-dependent drag *increases* (roughly linearly) with increasing extension if one is only considering *isolated* chains [27,32,33]. Thus in fact, the Giesekus model, based on *interchain interactions* as discussed above, does the exact opposite of what is necessary to correct the FENE-P model at large extension.

We conclude then by noting that using the Oldroyd-B model in flows where there are stagnation points with significant extensional character is fraught with difficulties since the model itself, even in multi-mode form, for $De > 1/2$ presents a stress singularity at steady state, and unbound exponential chain stretch as a function of Hencky strain. This stretch/stress singularity can be removed by introduction of chain finite extensibility through the pre-averaging approximation and/or through the addition of the *Giesekus* drag term via Eq. (32). However neither of these changes produce a quantitative model for large Hencky strain in extensional flow of a real polymer solution and care must be taken in interpreting the results.

2. Predictions of the Oldroyd-B model in elastic instabilities of viscometric flows with curved streamlines

The Oldroyd-B fluid model has played a central role in studies of elastic instabilities in simple bulk flows used for measurement of rheological properties of viscoelastic fluids. This class of shear flows also has significant practical implications in many polymer processing applications including single and multilayer film formation, coatings, and lubrication. To that end, the Oldroyd-B fluid model not only has been instrumental in discovery of fundamental physics that drives elastic instabilities in viscometric flows but also it has provided invaluable insight in flows of practical importance that exhibit elastic instability.

Studies in the past two decades have conclusively established that creeping flow of viscoelastic shear flows with curved streamlines undergo a purely elastic instability, see [34] for a review. Examples include Taylor–Couette [35–40], Dean and Taylor–Dean Flows [41–44], cone-and-plate and parallel plates flows [45–48]. The elastic instability in these flows occurs as a Weissenberg number, Wi, defined as the product of the fluid relaxation time to a shear rate as in Section 1.2, exceeds a critical value. Note in this context however that the definition of the Wi varied especially in the early literature (and in fact, at times it has been labeled as a *Deborah number)*, but careful examination demonstrates that all studies were essentially equivalent — elastic hoop stresses in curvilinear shear flows could drive elastic instability past a critical Wi that grew as the curvature became small at a fixed shear rate. Although, the complex spatio-temporal characteristics of the secondary flow and its *nonlinear* evolution depend on the flow geometry, the single and multi-mode Oldroyd-B (MMO-B) fluid have been successfully used not only to clearly elucidate that these purely elastic instabilities are essentially driven by the adverse gradient of elastic hoop stress across curved streamlines but also to qualitatively predict the critical Wi for the onset of the instability [34,37,39,40,49,50]. Experimental and theoretical studies of the effect of fluid inertia on linear stability and non-linear dynamics and pattern formation of this class of flows has also been examined by systematic variation of the Elasticity number defined as, $E = Wi/Re$ over up to three orders of magnitude, *i.e.,* $0 < E < 1$ to $E \gg 1$ [51–64]. To date, most theoretical studies have been conducted in the Taylor–Couette flow presumably due to the wealth of available experimental data. Specifically, the linear stability studies have been mainly based on the Oldroyd-B model while studies focused on non-linear dynamics and pattern selection have been conducted with the FENE-P model due to presence of highly localized structures in the post critical regime that give rise to strong elongational flows.

2.1. Taylor–Couette flow: Purely elastic and thermoelastic instabilities

Since the instabilities reviewed in this section occur in single phase inertialess bound flows of incompressible fluids, the *nonlinearity* inherent in the viscoelastic constitutive equation must be the sole driving force for occurrence of the instability/flow bifurcation. Hence, the single and multi-mode Oldroyd-B models are the natural starting point for theoretical analysis due to their ability to predict the shear rheology of Boger fluids commonly used in study of purely elastic flow transitions. In addition, the single mode model only has three material constants, the solvent and polymer viscosity as well as the longest

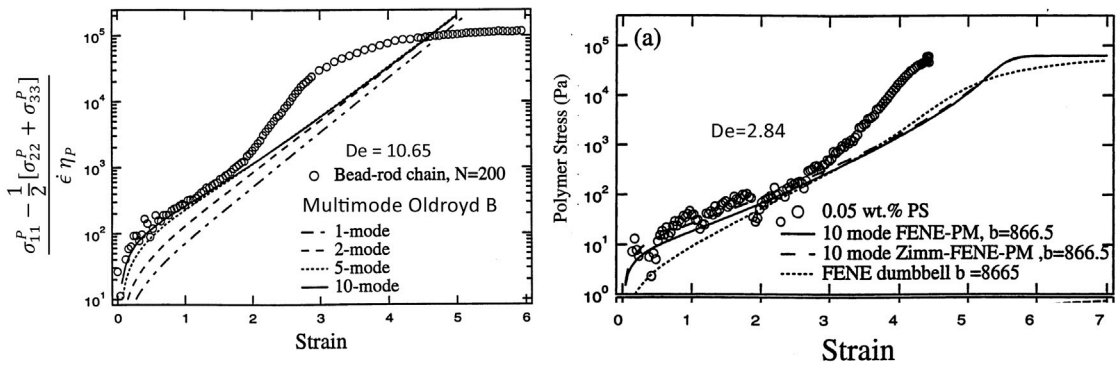

Fig. 2. (a) LEFT — Simulations of the polymer contribution to the extensional viscosity as a function of Hencky strain for a freely-jointed bead rod chain without hydrodynamic interactions and various multi-mode Oldroyd-B models. [27] (b) RIGHT — Extensional stress data from polystyrene "Boger" fluid as a function of Hencky strain compared to single and multi-mode FENE models. Note that in the figure, $\mathbf{b} = 3L^2/(N_k b^2)$ in the notation of the present article [27].

fluid relaxation time. This simplifies the linear stability analysis and facilitates mechanistic understanding of the instability phenomenon as well as comparison of theoretical predictions with experimental findings.

Giesekus in 1966 [65] observed a cellular instability in Taylor–Couette Flow (TC) of a polyisobutylene/decalin shear thinning solution at Reynolds number of approximately 0.01. Almost 20 years later, Muller, Larson, and Shaqfeh, experimentally demonstrated that above a critical Wi, the TC flow of a polyisobutylene Boger fluid transitions from a purely azimuthal shear flow to a banded vortex structure (see Fig. 3) at vanishingly small Reynolds number, *i.e.*, 0.001 [34,37,39,40]. The Wi in this context was defined as $Wi = \dot{\gamma}\lambda$ where $\dot{\gamma}$ is the shear rate in the small gap Couette cell, however, in this literature, it was referred to as a Deborah number, De. In addition, Larson et al. [39] showed that this flow transition occurs irrespective of the sole rotation of the inner or the outer cylinder; hence, providing clear evidence of the existence of a purely elastic instability in TC flow of dilute polymeric solutions. Moreover, the instability was reported to give rise to a *time-dependent* secondary flow.

Shortly after this discovery many Oldroyd-B based linear stability studies of viscoelastic TC flow were initiated. The initial analyses [37,39,40] assumed the instability mode to be *axisymmetric* partly due to experimental observations of the initial stages of the secondary flow by Larson et al. [39]; however, subsequent linear stability analyses by Avgousti and Beris [66] and Joo and Shaqfeh [41] unequivocally demonstrated that under isothermal conditions the most dangerous disturbance to the base flow is *non-axisymmetric* and *time-dependent* with a critical Wi of $O(10)$. Moreover, the mechanism of the instability based on energy analysis with the Oldroyd-B model [41] was determined to be due to the coupling of radial velocity fluctuations to finite hoop stresses that lead to amplification of the radial perturbations, and a *non-axisymmetric, oscillatory* secondary flow.

The eigenvalue problems describing the elastic TC flow instability in the small gap limit were particularly simple, and for example, for the axisymmetric mode discovered first [39] the eigenvalue problem becomes:

$$\phi'''' - 2\alpha^2\phi'' + \alpha^4\phi = -\epsilon Wi^2\alpha^2\Lambda\phi', \quad \phi(0) = \phi(1) = 0 \tag{33}$$

with ϕ the stream function of the perturbation in the gap of the TC flow, "prime" denoting differentiation with the gap variable, Λ the eigenvalue, α the axial wavenumber and ϵ the ratio of the gap thickness to the radius of the Couette cell. Thus the left hand side represents the viscous forces in the flow and the right hand side is the driving term associated with elasticity. The right hand side obviously depends on finite curvature through ϵ, and elasticity with the combined parameter ϵWi^2 being an *Elastic Taylor Number*. It drives the fluctuating viscous flow and has its origin in the terms $-\mathcal{L}_{ik}\sigma^P_{jk} - \mathcal{L}_{jk}\sigma^P_{ik}$ from the upper convected derivative. This fact, suggested the instability was a "hoop stress" instability through the Oldroyd-B model, with a fluctuating velocity gradient ϕ' acting on the existing hoop stresses in the base state to enhance the hoop stresses and reinforce the flow. As mentioned above, this was later verified rigorously via energy analysis [41].

Although early experimental observations [34,37,39,40,67] were qualitatively in agreement with the theoretical predictions based on the Oldroyd-B model, later detailed particle imaging velocimetry experiments conducted by Baumert and Muller [35,36] demonstrated that the primary flow transition leads to a secondary flow state composed of *axisymmetric* and *stationary* toroidal vortices, similar to those seen at the onset of instability in the Newtonian Taylor–Couette flow. Moreover, it was shown that the Wi_c is $O(1)$ [34,37,39,40,49].

Even a cursory perusal of the above summary of the primary flow transition in TC flow of dilute polymeric solutions reveals puzzling differences between experimental observations and theoretical predictions — differences that were highlighted by various experimental studies using different test fluids and cylinder radius ratio. First and foremost, the Baumert and Muller [35,36] experimentally measured Wi_c is approximately 10 times lower than the Oldroyd-B model predictions [34,37,39,40]. Secondly, the Oldroyd-B based analysis predicts spatiotemporal characteristics of the secondary flow that are in agreement with earlier experiments findings of Larson et al. [39] but are in stark contrast to the more detailed experimental observations of Baumert and Muller [35,36] that were subsequently reproduced by Groisman et al. [51]. Various explanations have been proposed to rationalize the disparities between experimental observations and Oldroyd-B theoretical predictions. Chief among them is the inability of the single mode Oldroyd-B model to predict the response of Boger fluids to transient shear and extensional deformations [68]. Predictions based on the MMO-B and the Multi-mode Giesekus (MMG) models that can adequately predict the transient shear and extensional deformations of Boger fluids indicate that although second normal stresses and shear thinning of first normal stress are stabilizing, the predicted critical Wi is still significantly higher than the experimentally measured Wi_c [69,70]. In addition, the spatio-temporal characteristics of the secondary flow is qualitatively the same as the single-mode Oldroyd-B model, *i.e.*, a *non-axisymmetric* and *time dependent* flow [69]. Moreover, symmetry considerations [63], local *nonlinear* analysis [64], and finite element time integration of the linearized equations [71] have further shown that the discrepancy between isothermal analyses and experiments of Baumert and Muller [35,36] and Groisman et al. [51] cannot be reconciled.

The influence of energetics on the stability of the viscoelastic TC flow could be significant since Boger fluids have a very high viscosity and large activation energies for the fluid viscosity and relaxation time ($\backsim$ 60 kJ/mol [68]). Hence, even a temperature change of the order of 1 °C across the gap can lead to significant inhomogeneities in the fluid properties, which in turn can induce changes in the hoop stress

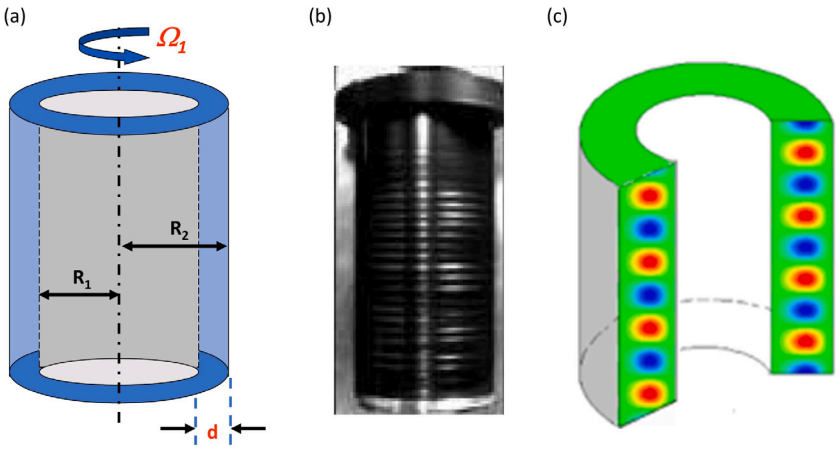

Fig. 3. Purely elastic instability in Taylor–Couette Flow: (a) The Taylor–Couette geometry with inner cylinder rotation; (b) Image of the secondary flow; (c) Schematic depiction of the banded vortex secondary flow structure [34].

gradient and Wi_c. In fact, the effects of viscous heating will always be present to some level *in the shear flow of highly elastic fluids with curved streamlines*, particularly, flows with closed streamlines in which the heat from viscous dissipation is accumulated in the device over long periods of operation. In fact, Arigo et al. [72] have experimentally demonstrated that viscous heating can lead to inhomogeneous temperature distribution in cone-and-plate and parallel-plate flows.

Motivated by the above-mentioned discrepancies and the plausibility of the existence of an inhomogeneous temperature distribution in this class of flows, Al-Mubaiyedh et al. [70,73] performed a linear stability analysis of viscoelastic TC flow that included viscous heating effects in a thermodynamically consistent fashion. Specifically, they modified the isothermal Oldroyd-B constitutive equation based on the principle of pseudo-time proposed by Crochet and Naghdi [74] to account for the fact that the stress–temperature relationship is not local, *i.e.*, the stress at any point depends on the fluid thermal history. Their analysis showed that depending on the ratio of the relaxation time to the thermal diffusion time, characterized by the ratio of Wi to the Peclét number, $Pe = \frac{d}{k/\rho C_p}(\frac{kd^2}{\eta_T R_1})$ ($d[\equiv R_2 - R_1]$, ρ, k, C_p, $\eta_T[\equiv \eta_s + \eta_p]$ are the gap size, density, thermal conductivity, specific heat capacity, pressure, and solution viscosity at the reference temperature, respectively), viscous heating could significantly influence the onset conditions and the selection of the most dangerous eigenmodes. Moreover, they discovered that viscous heating leads to a completely new type of viscoelastic instability, namely, purely thermoelastic instability ($Re \backsim 0$). The energy analysis indicates that mechanism of this instability is distinct from that of the purely elastic isothermal instability and arises from the convection of a base state temperature gradient by radial velocity perturbations. This in combination with the thermal sensitivity of the fluid gives rise to reduced dissipation and hence destabilization [75]. The secondary flow corresponding to the purely thermoelastic instability is *stationary* and *axisymmetric* with an $O(1)$ critical Wi. Subsequently, White and Muller [76,77] experimentally validated these findings by demonstrating that in the presence of viscous heating the viscoelastic TC instability indeed occurs at $O(1)$ Wi_c and the primary flow transition is always to a *stationary* and *axisymmetric* flow state. However, it should be noted that this favorable comparison is not conclusive as a direct comparison between the experimentally observed flow transition and theoretical predictions is validated only after a *nonlinear* stability analysis is performed to ascertain the stability of the bifurcating solution. To that end, Al-Mubaiyedh et al. [78] utilized direct time-dependent simulations to examine the *nonlinear* evolution of finite amplitude disturbances of the purely thermoelastic instability in the postcritical regime. This analysis revealed that over a wide range of parameter space that includes the experimental conditions of White and Muller [76] the primary bifurcation is *supercritical* and leads to a *stationary* and *axisymmetric* toroidal flow pattern. The consistency of this theoretical finding with experimental results can be viewed as a *triumph of the non-isothermal Oldroyd-B model* in capturing the underlying physics of this complex flow transition. Finally, it should be noted that the onset time associated with the evolution of finite amplitude disturbances to the secondary flow state is comparable to the thermal diffusion time. Hence, the time required to experimentally observe the secondary flow state is highly dependent on the thermal diffusivity of the test fluid and cylinder radius ratio. This observation could be the rationale behind the above-mentioned discrepancy between different experimental observations.

2.2. Taylor–Couette flow: Inertial effects and pattern formation

The Oldroyd-B model has also been used to examine the effect of inertia on the linear stability of viscoelastic TC flow by Joo and Shaqfeh [79], and Avgousti and Beris [66]. These studies have demonstrated that inertia destabilizes the elastic TC flow if only the inner cylinder is rotated, while it stabilizes the flow when only the outer cylinder is rotated. Joo and Shaqfeh [79] have also determined the mechanism of this stabilization and destabilization phenomenon based on an energy analysis. The analysis reveals that elastic forces are destabilizing in both modes of operation. Hence, the Reynolds stresses are mainly responsible for this phenomenon, namely, in case of inner cylinder rotation, the Reynolds stresses produce energy, therefore are destabilizing, while for the outer cylinder rotation, the Reynolds stresses dissipate energy, thus are stabilizing. The predicted destabilizing effect of inertia is consistent with experimental findings despite the fact shear thinning effects complicate the precise measurement of the critical E for flow instability [36,52]. It should be noted this favorable comparison can be viewed as another example of *the success of the Oldroyd-B model*.

The non-isothermal Oldroyd-B fluid has been also been used to ascertain the influence of fluid inertia on the onset of thermoelastic instability in TC flow by Thomas et al. [80]. Despite the large parameter space of the non-isothermal stability analysis, *i.e.*, (Re, Pe, Wi), the systematic analysis of Thomas, Sureshkumar and Khomami have conclusively determined that similar to the isothermal case, inertia destabilizes the flow when the flow is driven by the rotation of the inner cylinder. These findings are also consistent with experimental findings of [81].

Comprehensive experimental studies of non-linear dynamics and pattern formation in viscoelastic TC flow began in the late 90s by Steinberg and Groisman [55] and Baumert and Muller [57]. Their

detailed flow visualization studies with Boger fluids as well as shear thinning dilute polymeric solutions revealed novel flow patterns in the post-critical regime of inertial $E < 1$ and elastically dominated flows $E \gg 1$ flows, namely, rotating standing waves *(RSWs)* or *ribbons*, *disordered oscillations (DOs)*, *oscillatory strips (OSs)*, and *diwhirls (DWs)*. In addition, a very intriguing non-axisymmetric *flame pattern* that results from merging of nearby *DW-like* coherent structures (CS) was observed at low and high elasticity numbers. Kumar and Graham [58,59] took the first significant step toward understanding pattern formation in viscoelastic TC flow via *two dimensional steady-state spectral simulations* with the FENE-P model, albeit with a low chain finite extensibility, *i.e.*, $L \sim 43$. Their simulation captured the existence of a spatially localized CS similar to the experimentally observed *DW* patterns.

As evident from the above discussion, three-dimensional and time-dependent simulations are necessary to theoretically determine the pattern selection in the postcritical regime. Specifically, as demonstrated by Thomas, Sureshkumar and Khomami [61], three-dimensional transient simulations that allow for the computation of symmetry breaking of inflow/outflow (I/O) of an ideal *RSW* are required to capture flow transitions that lead to the formation of localized solitary vortices that exhibit narrow regions of strong inflow surrounded by broad regions of weak outflow. To that end, Thomas, Sureshkumar and Khomami [62] performed the first successful three-dimensional and time-dependent simulations of viscoelastic Taylor–Couette with the FENE-P model with $L = 100$ using a hi-fidelity fully implicit parallel spectral time-splitting algorithm and discovered flow patterns with various spatiotemporal symmetries, namely rotating standing waves *(RSWs)*, disordered oscillations *(DOs)* and solitary vortex structures referred to as oscillatory strips *(OSs)* and diwhirls *(DWs)*. Specifically, for $E > 0.1$ when the shear rate (inner cylinder rotation speed) increased above the linear stability threshold, the circular Couette flow *(CCF)* becomes unstable to *RSWs* implying symmetry between inflow/outflow (I/O) regions. Further increase in the shear rate leads to the I/O symmetry breaking and appearance of *DOs* and/or *flame-like* patterns with spectral mechanical energy transfer similar to that of *elastically induced low-Reynolds-number turbulence* (see Fig. 4). However, when the shear rate is decreased from this chaotic state, the radially inward polymer body force produced by flow-induced molecular stretching leads to the development of narrow inflow regions surrounded by much broader weak outflow domains. This promotes the formation of solitary vortex structures, which can be stationary and axisymmetric *(DWs)* or time-dependent (OSs) that mainly result from merging of vortex pairs. Finally, as the shear rate is decreased further, *DWs* decay to *CCF* flow at values of the Wi smaller than the linear stability threshold (see Fig. 4). These hysteretic flow transitions with respect to variations in the Wi as well as the above-mentioned predictions of various flow states compare very favorably with experimental observations [55,57].

2.3. Taylor–Couette flow: Elastic turbulence

Groisman & Steinberg [82] experimentally discovered a flow state with broad temporal frequency spectra in TC flow of dilute solutions in the limit of vanishing Re and $Wi_c \sim 5$, *i.e.,* extremely large E, dubbed "elastic turbulence" (ET). Specifically, they observed a broad frequency spectra in the radial velocity with two power-law decay regimes of slope -1.1 and -2.2 at low and high frequencies, respectively. In addition, it was shown that the probability density function (PDF) of the radial velocity at the middle of the gap exhibited a weakly asymmetric shape instead of the Gaussian distribution observed in inertial turbulence of TC flow. Thus, due to the steep decay of the velocity spectrum, ET is essentially a spatially smooth and temporally random flow, dominated by strong nonlinear interaction of a few large-scale spatial modes that give rise to $O(1)$ drag enhancement [83].

Numerical simulations of an elastically driven flow transition at vanishing Re and $O(1)$ values of the Wi, have been performed by Berti et al. [84,85] in a "toy" flow with the Oldroyd-B fluid model. These 2-dimensional simulations qualitatively capture the experimental findings of Groisman and Steinberg [82,86,87], however, quantitative differences exist between the simulation results and experiment. The authors have attributed these discrepancies to the approximate nature of the simulated flow and its two-dimensionality. In addition, these simulations lack the detailed flow–microstructure coupling needed for elucidating the mechanism of elastically induced turbulence. To that end, Liu and Khomami [88] performed the first DNS of elastically induced turbulence for $0.2 \leq E \leq 5$. These simulations capture the key features of elastically induced turbulence, namely, the broad continuous power-law-decay regions spanning more than two orders of magnitude in frequency with two power-law decay slopes of -1.1 and -2.2, an asymmetric PDF of the radial velocity at the middle of the gap, and drag enhancement (see Fig. 5 for a direct comparison of DNS results and experimental findings). Although the aforementioned simulations capture the key experimental observations of purely elastic turbulence, particularly at $E \geq 1$, DNS of purely elastic turbulence, *i.e.,* in the limit of extremely large E remains a grand challenge problem for the research community engaged in developing first-principle models and simulations that can predict faithfully the complex spatio-temporal dynamics of polymeric flows.

2.4. Dean and Taylor–Dean flows

Shortly after the "discovery" that a purely elastic instability was present in TC flow as driven by hoop stresses, the question naturally was posed as to whether other curvilinear shear flows would also be unstable to cellular instabilities as driven by hoop stresses. Following the literature then in inertially driven instabilities, Joo and Shaqfeh demonstrated that planar Dean flow (i.e. pressure driven flow around a curved channel) was subject to purely elastic instability and, moreover, when combined with shear driven flow, i.e. Taylor–Dean flow, new elastic instability modes were present [42,43]. Again, the analysis started with the Oldroyd-B equation. This analysis was important and unique for at least two reasons: (1) the mode of elastic instability driven by the parabolic flow was different and was characterized by a different modal structure (e.g. stationary, axisymmetric) and (2) combinations of pressure and shear driving force around curved streamlines are present in a host of practical flows beyond rheometry, e.g. bearing flow, and thus this result implied the practical implications of the growing body of research regarding the stability of elastic shear flows with curved streamlines. Again, in the small gap limit of these Taylor–Dean flows, for the axisymmetric mode, the eigenvalue problem (in terms again of the stream function in the flow-gradient plane), takes a simple form that is informative [42]:

$$\phi'''' - 2\alpha^2\phi'' + \alpha^4\phi = -\epsilon Wi^2\alpha^2\Lambda_1\phi' - \epsilon Wi^2\alpha^2\Lambda_2\phi, \quad \phi(0) = \phi(1) = 0 \quad (34)$$

where Λ_1 and Λ_2 are functions of the eigenvalue. In this context the Weissenberg number again referred to as a Deborah number in this literature, was defined as the product of the *maximum* shear rate across the gap times the relaxation time. If we compare this to the small gap limit of the TC flow, Eq. (33), we note that the second term on the right hand side is new. It comes from the substantial derivative in the upper convected derivative, i.e. $u_k \frac{\partial \sigma^p_{ij}}{x_k}$, and, in fact, drives a new stationary instability mode [42,43]. Energy analysis of this mode [42] demonstrated that the mode was driven by a *velocity fluctuation ψ acting on the normal stress gradients in the base state*. Again, all of these conclusions stemmed from analysis of the Oldroyd-B model. Moreover this new mode of instability scaled with the same parameter ϵWi^2 as that characterizing the elastic TC instability, although in this context, it can be referred to as an *Elastic Dean number*. For flows with both shearing and pressured driven components, the two separate modes associated with the TC flow and Dean flow are present and the most unstable depends on the relative strengths of each flow driving force [42]. All of these instabilities were examined in the laboratory [41] although again the

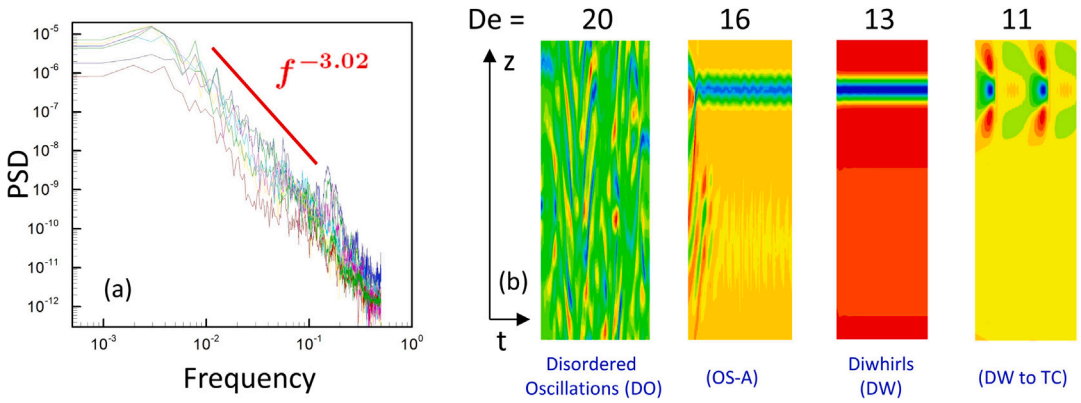

Fig. 4. (a) Power spectral density of the radial velocity component as a function of dimensionless frequency at two positions close to the middle $(R_1 + R_2)/2$ of the gap, (b) Space–Time Plots of the Radial Velocity (Blue-Inflow, Red-Outflow) at middle of the gap; $E = Wi_c/Re_c = 1/3$; $Re/Re_c = 0.9$ [62].

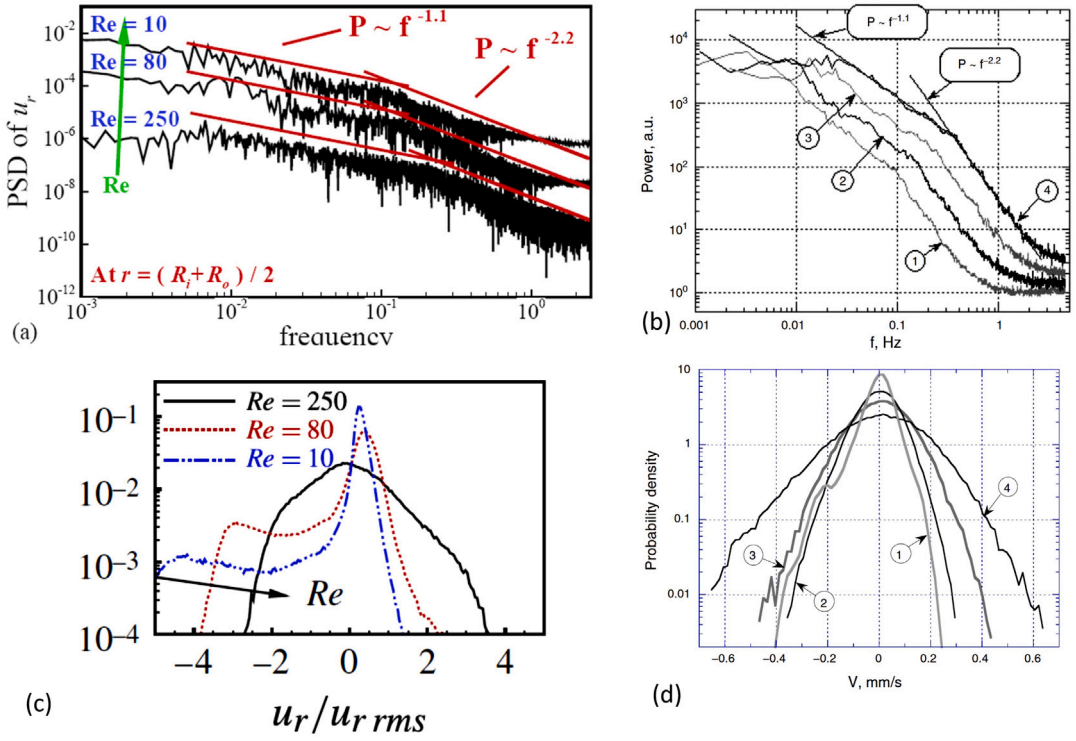

Fig. 5. Power Spectral Density (PSD) of radial velocity fluctuations as a function of frequency at the middle of the gap at $Wi = 50$ (a) DNS, (b) Experiments, curves 1–4 correspond to $Wi = 8.5$, 13.6, 21.8 and 35, respectively; Probability density functions (PDF) of the radial velocity at the middle of the gap at gap (c) DNS at $Wi = 50$ (d) Experiment, curves 1–4 correspond to the same Wi in (b).

predictions from the Oldroyd B model of the onset conditions and the wavelength of the cellular instability were qualitative not quantitative. Moreover, subsequently, eccentric cylinder flow or bearing flow was also examined within the context of the Oldroyd-B model. Indeed the flow is elastically unstable to a cellular instability very similar to that of the Taylor–Dean family [89–91].

Much less subsequent work has been done on the Taylor–Dean class of elastic instabilities (in terms of nonlinear analysis and simulation) as compared to Taylor–Couette flow. Fan et al. [92] completed elastic flow computations for fully, developed curved pipe flow, where the Oldroyd-3-constant model was used to represent the viscoelastic fluid and this includes the upper-convected Maxwell (UCM) model and the Oldroyd-B model as special cases. Interestingly, they found an upper bound on the Deborah number, defined as $De = \frac{\lambda U_m}{a}$ where a is the pipe radius and U_m is the mean velocity in the pipe, beyond which no steady solution could be found. This "critical" Deborah number obeyed the same relation for different values of the pipe curvature $\mathcal{R}$ as suggested by the elastic Dean number in the Joo & Shaqfeh stability analysis, namely, for

$$\left[\frac{a}{\mathcal{R}}\right]^{1/2} De \geq \left[\left(\frac{a}{\mathcal{R}}^{1/2}\right) De\right]_{crit}$$

no steady solutions could be found. In addition, Zilz et al. [44] examined the pressure driven flow in a serpentine rectangular channel, and demonstrated that an elastic Dean number did correlate with the onset of cellular instability for different channels. (Note the elastic Dean number is one of the class of Pakdel–McKinley numbers [93] as discussed below, and [44] expressed the geometric dependence of the critical conditions in that language.) In this same paper, calculations of the cellular flow in the serpentine channel are made using the Maxwell model, and the onset to a cellular instability was indeed found where the onset conditions were in good agreement with the numerical simulations.

The influence of energetics on the linear stability of viscoelastic Dean flow of an Oldroyd-B liquid was investigated by Al-Mubaiyedh et al. [94]. This was briefly mentioned above in the discussing energetics of the TC flow. Interestingly the analysis showed that when the temperatures of inner and outer walls are maintained at constant equal values, viscous heating does not influence the mode selection, i.e. the most dangerous disturbance is axisymmetric and stationary as in the case of isothermal Dean flow. The critical Weissenberg number does increase with increasing Brinkman number indicating that viscous heating stabilizes the flow in this case.

2.5. Cone-and-plate and coaxial parallel-plate flows: Purely elastic and thermoelastic instabilities

The torsional flow between coaxial parallel plates and a cone-and-plate are pervasive in rheological characterization of viscoelastic fluids. Hence, determining the critical conditions for flow transitions is these torsional flows is of utmost importance for accurate measurements of fluid viscosity and normal stresses. In fact in the mid 80s, appearance of curious time dependent phenomenon at a critical shear rate, namely, amplification of oscillations of torque and thrust force with time in a dilute polymeric solution was interpreted as a sign of a change of rheological properties of the fluid [95]. Later it was postulated that these changes occur due to formation of a shear induced network and the phenomenon was dubbed *anti-thixotropy* [96].

Larson and Magda [45] experimentally reproduced this phenomenon with dilute polymeric solutions in both of these torsional flows; however, they ascribed it to occurrence of a purely elastic instability discovered earlier by Phan-Thien [97,98]. Specifically, Phan-Thien had carried out an analytical stability analysis with the Oldroyd-B fluid model in the limit of long-wavelength disturbances using the von Kármán similarity form. Remarkably the predicted critical Wi for both geometries only depended on S, defined as the ratio of solvent to the total viscosity (Note that $S = \beta$ as defined in the introductory section of this article and is now generally used in this context). Almost two decades later the precise β and geometry dependence of the critical Wi for the cone-and-plate flow was determined by Olagunju [99,100].

McKinley et al. [46] performed the first flow visualization experiments of a PIB/PB Boger fluid in a cone-and-plate geometry to ascertain the existence of a purely elastic instability at a critical Wi. As seen in Fig. 6 above a critical Wi, indeed an instability is manifested in the form of Bernoulli spirals that propagate outwards. This nonaxisymmetric flow transition was shown to be *overstable* in time and *subcritical* in shear rate. These experimental observations contradict the long wavelength solution of Phan-Thein but are in qualitative agreement with Olagunju's [99,100] results obtained in the small gap limit and/or based on a short wavelength perturbation analysis. Specifically, these analyses show that the instability is of finite wavelength and does not solely depend on β, but it also depends on the square root of the cone angle.

The first linear stability analysis of the viscoelastic cone-and-plate flow was performed by McKinley *et al.* [48] with the Oldroyd-B and Chilcott–Rallison constitutive equations, and later by Öztekin *et al.* [101] based on a 4-mode Giesekus model with parameters determined by fitting the rheological data of the test fluid. These analyses revealed that incorporation of shear thinning and a spectrum of relaxation times is essential to quantitatively predict the critical Wi for the onset of the instability and the secondary flow state. It is important to note that *the effect of the free surface* on the instability of the cone-and-plate flow had yet to be investigated. We note also that in this literature, McKinley and coworkers defined a Weissenberg number, $Wi = \dot{\gamma}\lambda$ and a Deborah number, $De = \Omega\lambda$ where Ω is the angular frequency of rotation of the cone, and presented their stability criteria in terms of a critical value of the product $WiDe$. A bit of algebra demonstrates that this is completely equivalent to the Elastic Taylor and Dean number criteria as discussed above for TC flow and Dean flow.

Byars *et al.* [47] performed extensive flow visualization studies of the coaxial plate and plate flow using two Boger fluids with two different aspect ratios, defined as the plate radius divided by the plate separation distance. These studies conclusively demonstrated that above a critical Wi a set of radial vortices appear within the gap (see Fig. 6). Moreover, they observed a spatial pattern at a finite radius envelope for a given Wi in the form of concentric rings or a nested Archimedean spiral that propagates outward.

Öztekin and Brown [102] performed a local linear stability analysis of the coaxial plate and plate flow using the Oldroyd-B fluid model. This analysis correctly predicted that above a critical Wi the torsional flow transitions to a nested Archimedean spiral flow pattern; however, the finite envelope nature of the radius mentioned above was not captured by the analysis. In turn, Byars *et al.* [47] extended the Oztekin & Brown [102] analysis by taking into account the effect of shear thinning of the first normal stress by performing a local linear stability analysis with the Chilcott–Rallison model. The analysis demonstrated the importance of the shear thinning of the normal stress in predicting the finite envelope of unstable values of the critical radius for a given Wi. This observation can be rationalized based on the radial dependence of hoop stresses. Specifically, at a given Wi, one has to move outward from the center to a critical radius where the base state hoop stresses become large enough to trigger a purely elastic instability. However, at an even a larger distance from the center of the plates, the fluid begins to shear thin. This plus the fact that the radius of curvature increases linearly with distance from the center of the plates leads to a reduction in hoop stresses and flow restabilization. This analysis not only correctly predicts the onset conditions and their localized radial nature but also captures the secondary flow structure in concert with experiments, namely, nested spiral vortices that propagate outward. The presence of a free surface at the edge of the parallel-plate geometry was later included in a finite domain linear stability analysis by Avagliano and Phan-Thien based on the Oldroyd-B model. [103,104]. The agreement between the analysis and experiments is improved when the edge effects that drive a weak secondary flow are included in the analysis. This is an important finding as it demonstrates that *the weak secondary flow generated by the free surface at the edge plays an important role in the finite envelope nature of the critical radius in the incipient secondary flow* as the Oldroyd-B model cannot capture the shear thinning of the first normal stress that has been considered critical in capturing this phenomenon. Later, Renardy and Renardy [105] inspired by the analytical model developed by Olaganju [106], were able to closely approximate the two-dimensional numerical results of Avagliano and Phan-Thien [104].

It is perhaps not surprising in retrospect that the mechanism of both the coaxial parallel plates and cone-and-plate instabilities is essentially the same as that predicted by Larson *et al.,* in 1990 for the viscoelastic TC flow [39], *i.e.,* coupling of radial velocity fluctuations to finite hoop stresses. Pakdel and McKinley [93] used this fact to develop a general criterion, based on dimensional analysis arguments that is capable of estimating the occurrence of elastic instabilities in a broad range of isothermal, single phase viscoelastic flows. Since, the "Pakdel–McKinley number (PM)" is based on a measure of elastic stresses and the characteristic radius of curvature of the flow, it contains the essential ingredients that drive purely elastic instabilities in flows with curved streamlines. The basic argument is as follows and starts from the properties of the Oldroyd-B fluid. If a broad class of curvilinear shear flows are subject to purely elastic instability, then they can all be characterized by a critical value of the elastic Taylor number based on local conditions — or in the previous notation, a critical value of:

$$PM_{crit} = \left[\frac{\lambda U}{R}\frac{\sigma_{11}^{p}}{\eta_T \dot{\gamma}}\right]^{1/2} \tag{35}$$

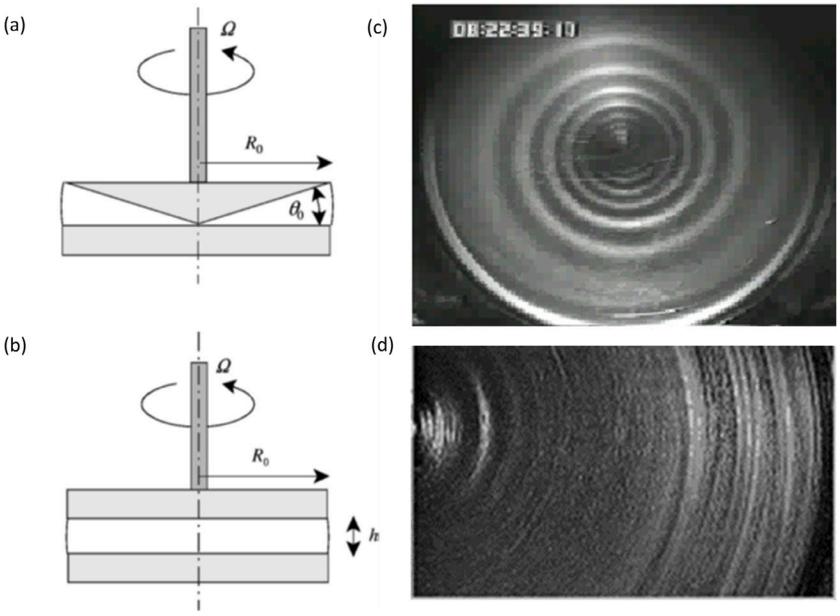

Fig. 6. Purely elastic instability in cone and plate and coaxial Parallel Plate Flows: (a) The cone and plate geometry with a rotating cone (b) The parallel plate geometry with a rotating upper plate; (c) Image of the secondary flow in the cone–plate geometry [46] (d) Image of the secondary flow in the parallel plate geometry [46].

where U is the local flow velocity, σ_{11}^p is the local polymer normal stress along the flow direction, R is a local radius of curvature, and $\dot{\gamma}$ is a local shear rate. This corresponds to making the relaxation time in the second term in the product that is the elastic Taylor number $\epsilon Wi * Wi$ equal to $\frac{\sigma_{11}^p}{2\eta_T\dot{\gamma}^2}$ (which is proportional to the relaxation time in the Oldroyd-B model) and then taking the square root. Hence, it is not too surprising that despite the fact that the numerical value of the PM cannot be computed based on scaling analysis, the scaling predicts the occurrence of purely elastic instability in Taylor–Couette, and cone-and- plate flows, as well as flow between eccentric rotating cylinders. The advance here is that this criteria can be used even if it is not obvious at all that the Oldroyd-B captures σ_{11}^p. While PM cannot capture the critical Wi for a particular flow or the spatio-temporal characteristics of the secondary flow, nor can it distinguish between purely elastic instabilities in pure shearing or mixed kinematic flows where extensional stresses play an important role in determining the stability of the flow, it provides a simple and useful means for determining if a complex flow is prone to purely elastic instabilities.

Rothstein and McKinley [107] have performed a comprehensive experimental study of the effect of viscous heating on the torsional steady shearing of monodisperse polystyrene dilute solutions realized in a cone-and-plate and coaxial parallel plates. The experimental results are presented in terms of the Wi, and the Nahme–Griffith number, $Na = \frac{\eta_0 H^2(\Delta H/RT)\dot{\gamma}}{kT}$ (where η_0 is the zero shear viscosity and R is the universal gas constant) that measures the magnitude of viscous heating. More importantly, they demonstrate that the importance of these two competing effects can be quantified via a thermoelastic number, defined as $\Theta = \lambda R_0\sqrt{\frac{\eta_0(\Delta H/RT)}{kT}}$ (where λ is the polymer relaxation time, and R_0 is the plate radius), that allows viscoelastic instability in different fluids and flow geometries be presented in a single stability diagram. Using this elegant methodology, the thermoelastic number was systematically changed by variation of the temperature of the test fluid or the configuration of the test geometry. These comprehensive experiments clearly demonstrate that when the characteristic time scale for viscous heating is much longer than the relaxation time of the test fluid ($\Theta \ll O(1)$) the critical conditions for the onset of the elastic instability are in good agreement with the predictions of isothermal linear stability analyses. As the thermoelastic number approaches a critical value, the strong temperature gradients induced by viscous heating reduce the elasticity of the test fluid and delays the onset of the instability. At even larger values of the thermoelastic parameter $O(10^{-1})$, viscous heating stabilizes the flow completely. Overall, these results are consistent with earlier theoretical findings of Al-Mubaiyedh, Sureshkumar, and Khomami [94] obtained based on a thermodynamically consistent non-isothermal Oldroyd-B model in the Taylor–Dean flow. Thus, the dominant mode of the instability does not change in presence of viscous heating, but the critical Wi for the onset of the instability is increased. It should also be noted that the thermoelastic mode is still present in the Taylor–Dean and torsional flows but it does not become dominant until much higher Pe than those observed in the non-isothermal viscoelastic TC flow. These results along with the detailed mechanistic analysis of Al-Mubaiyedh *et al.*[94] indicate that the critical Pe at which the thermoelastic instability manifests is dependent on the symmetries of the base flow.

2.6. Cone and plate and coaxial parallel plates flows: Non-linear stability analysis

Unlike the viscoelastic TC flow, the non-linear dynamics of torsional elastic flows is essentially unexplored with the exception of Olagunju's [108] weakly nonlinear stability analysis for the viscoelastic cone-and-plate flow in the limit of small cone angle. This Oldroyd-B based analysis reveals that β has a very pronounced effect on the solution bifurcation. That is for $\beta > 0.02$, *i.e.,* the small solvent viscosity limit, a subcritical Hopf bifurcation in shear rate is observed. However, for $\beta < 0.02$ the flow transition is supercritical. The good agreement between the theoretical and experimental observations of McKinley [46,48] in the limit of small cone angle can be viewed as yet *another success of the Oldroyd-B model.*

3. Polymer induced turbulent drag modifications as predicted by the Oldroyd-B model

It is well known that the addition of small amounts of soluble high molecular weight polymers to inertia-dominated, wall bounded flows gives rise to a modification of turbulent drag. Specifically, the addition of minute amount of long chain polymers to rectilinear, unidirectional wall-bounded turbulence leads to a dramatic decrease in turbulent friction drag (DR), which saturates at 80% reduction, at the so called

maximum drag reduction (MDR) asymptote [109–111]. In contrast, addition of a small amount of polymer to inertially-dominated curvilinear flows such as TC flow results in significant drag enhancement (DE). In what follows, the influence of the addition of trace amount of polymers on drag modifications of pressure driven channel flows, namely, plane Poiseuille flow, as well as TC flows will be discussed. The review will be focused on DNS of these flows, punctuated with experimental findings that have been essential to the mechanistic understanding of the influence of polymer additives on flow dynamics and drag modification.

3.1. Polymer induced drag reduction in plane Poiseuille flow

The development of hi-fidelity numerical techniques for DNS of viscoelastic turbulent flows in the past three decades has enabled the investigation of turbulent drag reduction in dilute polymer solutions using kinetic theory based constitutive equations. To date, DNS studies have played a crucial role in understanding the interplay between polymer chain dynamics, *i.e.*, extensional viscosity, relaxation time and polymer stress, and flow dynamics, namely, turbulent fluctuations and coherent structures. In fact, DNS studies have been essential in mechanistic understanding of polymer induced turbulent drag modifications, particularly in light of the lack of experimental techniques to precisely measure the elastic body forces that drive polymer induced and/or modification of turbulent dynamics.

DNS studies of turbulent channel flows with the Oldroyd-B model have been very limited presumably due the dominant nature of biaxial extensional flow regions between the streaks, thus, necessitating the use of constitutive equations with bounded extensional viscosity [112]. A noted exception is the DNS studies of Joseph and co-workers [113] based on the Oldroyd-B model aimed at understanding the mechanism of onset of polymer induced DR in turbulent channel flows. This study not only successfully predicted the $O(1)$ critical Wi for onset of DR in concert with experimental findings [114], but also sheds light on the mechanism that gives rise to the onset of DR based on the elastic theory of Taber and de Gennes [115]. To that end, it was shown that the polymer chains store elastic energy from the flow very near the wall and if this stored energy is released in the same region which occurs at low Wi, DR is not observed. Conversely, they demonstrated when the Wi reaches a critical $O(1)$ value, the elastic energy stored in the very near-wall region is transported to and in turn released in the buffer and log layers, showing low to modest drag reduction. The maximum DR realized in these simulations *i.e.,* $\sim$ 30% is in the low drag reduction regime (LDR) where the viscoelastic flow has similar statistical characteristics as the Newtonian flow and the mean velocity profile remains parallel to that of the Newtonian flow with an upward shift of the log-region that is enhanced as DR is increased to 30%–40%. Moreover, the streamwise velocity fluctuations are enhanced, while the transverse ones are reduced with increasing DR. Despite the limitations of these simulations to the LDR regime, presumably due to the inability of the Oldroyd-B model to capture a bounded extensional viscosity, the favorable comparison of the onset Wi and the mechanism leading to LDR with experiments and more comprehensive studies performed with constitutive equations that exhibit bounded extensional viscosity [116–118] is yet another example of *triumph of the Oldroyd-B model* to capture the complex polymer induced flow phenomena.

In addition to the LDR regime, experimental studies have identified a high drag reduction (HDR)) regime [119–121]. In this regime, (40% < DR < 60%), the slope of the mean velocity profile is dramatically changed as the slope of the log-law is significantly enhanced with increasing DR. In addition, the Reynolds shear stress becomes relatively small. At MDR the Reynolds shear stress becomes extremely small and the slope of the log-law region reaches the Virk asymptote.

Initial DNS studies, pioneered by Beris and co-workers [116] with the FENE-P model demonstrated that the extent of DR is a strong function of the fluid rheology, *e.g.,* the fluid relaxation time and the maximum chain extensibility [122–125]. Overall, these studies demonstrated that DR and the accompanying flow modification in the LDR regime, namely, the $O(1)$ value of Wi for onset of DR, the mean velocity profile, rms velocity fluctuations and the average spacing between the streamwise streaks can be predicted in excellent qualitative agreement with experimental findings. In addition, a few DNS studies successfully captured the formation of highly correlated and elongated streamwise low-speed streaks and the rapid reduction in the Reynolds stresses in the HDR regime as observed experimentally [117,126,127]. However, as shown by Li, Sureshkumar and Khomami [118], most of these predictions were made with computational domains that were not sufficiently long to accurately capture the dynamics of the flow in the HDR and MDR regimes (see Fig. 7a). To that end, Li *et al.,* [118] were the first to demonstrate that to accurately capture key features of the flow dynamics in the HDR and MDR regimes (see Figs. 8 and 9), very long computational domain lengths of the order of 10^4 wall units (see Fig. 7a), large polymer chain extensibility, L, and high Wi are required (See Fig. 7c). Evidently, the level of drag reduction tends to asymptote at large L and Wi. The shape of curves in Fig. 7c suggest that the influence of L and Wi can be decoupled. To this end, Li *et al.,* [118] developed a relationship for %DR as a function of $Wi_\tau = \lambda(\tau_w/\rho)/\nu_0$, L, and $Re_\tau = h(\tau_w/\rho)^{0.5}/\nu_0$, where h, τ_w, ρ, ν_0, and λ are the channel half height, wall shear stress, the density, the zero shear rate kinematic viscosity, and the relaxation time of the solution, respectively,

$$\%DR = 80[1 - e^{-\alpha(Wi_\tau - Wi_{\tau,c})(Re_\tau/Re_{\tau,r})^{-0.225}}][1 - e^{-\gamma L}] \tag{36}$$

where $\alpha = 0.025$, $\gamma = 0.0275$. $Wi_{\tau,c}(= 6.25)$ is the onset friction Weissenberg number. $Re_{\tau,r}$ is the reference friction Reynolds number, and it is set to $Re_{\tau,r} = 125$. The prefactor of 80 is used because at high Wi_τ and large L, the %DR at MDR asymptotes to 80% at high Reynolds numbers [111] . This relationship explicitly shows that effective drag reduction requires large polymer extensibility L and high Wi_τ number. Li *et al.,* [118] simulations also indicate that almost the same level of drag reduction can be obtained with FENE-P at $L^2 = 14{,}400$ and the Oldroyd-B ($L^2 \longrightarrow \infty$) models. This demonstrates that only at high $Wi_\tau \geq 100$ and high maximum chain extensibility can MDR be reached. A close examination of the figure indicates that this scaling accurately describes the extent of DR in the HDR and MDR regimes. However, in the LDR regime deviations are observed. This suggests that perhaps in this regime (*i.e.*, relatively small L values) the influence of L and Wi_τ cannot be decoupled.

Li *et al.,* [118] also observed that at large L^2 from the onset of DR to the MDR regime, $Wi = Wi_\tau(\omega^+_{x,rms})_{peak} \sim O(1)$ in the near wall region. This suggests that there is an intricate balance between elastic forces and average rotation speed of the near-wall axial vortices that is a measure of the average time between upwash and downwash events and Reynolds stress production. As shown below these findings are crucial to the mechanistic understanding of MDR.

The above-mentioned studies of polymer induced drag reduction in plane Poiseuille flow have established the mechanism by which polymers alter turbulence and give rise to DR from the onset to the HDR regime. Specifically, it has been shown that polymers suppress turbulence by counteracting velocity fluctuations in the wall normal and transverse directions. That is, the modification of near wall quasi-streamwise vortices leads to substantial polymer forces and torques that inhibit vortical motion leading to reduction of Reynolds stress production (see Fig. 10).

In addition, it has conclusively been demonstrated that in the LDR and HDR regimes, polymers extract energy from the flow as they are pulled around the near wall vortices either by upwash or downwash flows. In turn, polymers release energy back to the flow in the high speed streaks ($y^+ \sim 5$) and as a result enhance streamwise momentum [117,118,126,127] (see Fig. 11).

Until a decade ago, mechanistic understanding of MDR was one the most debated topics in viscoelastic unidirectional parallel shear

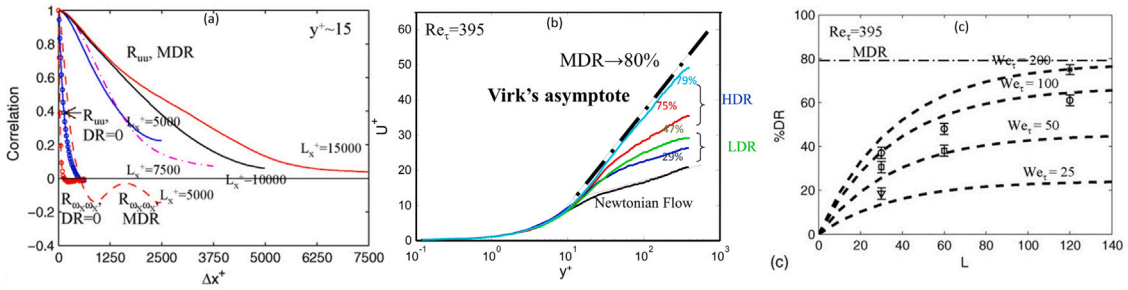

Fig. 7. (a) The influence of domain size on computed results in the MDR regime, streamwise two-point correlations (i.e., R_{uu} and $R_{\omega x \omega x}$) in the buffer layer; (b) Mean streamwise velocity profiles as a function of distance from the wall at friction Reynolds number, $Re_\tau = hU_\tau/\nu_0 = 395$ where $U_\tau = (\tau_w/\rho)^{0.5}$ is the friction velocity, τ_w is shear stress at the wall; (c) The influence of polymer chain extensibility, L, and friction Weissenberg number, $Wi_\tau = \lambda U_\tau^2/\nu_{P0}$ on the extent of drag reduction [118].

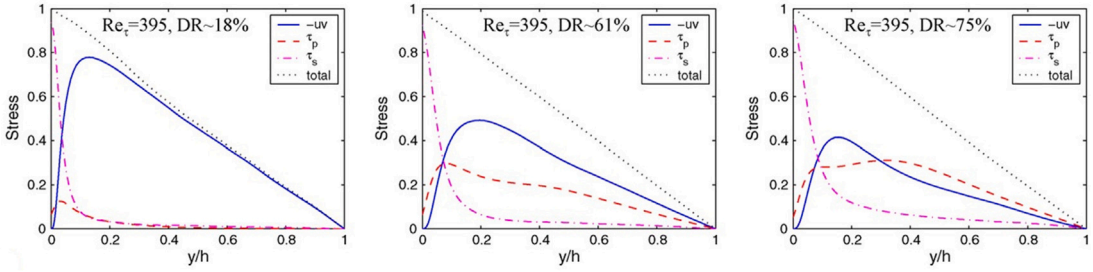

Fig. 8. Overall momentum balance as a function of the extent of DR at $Re_\tau = h(\tau_w/\rho)^{0.5}/\nu_0 = 395$. Reynolds stress $-uv$, polymer stress τ_p, solvent stress τ_s [118].

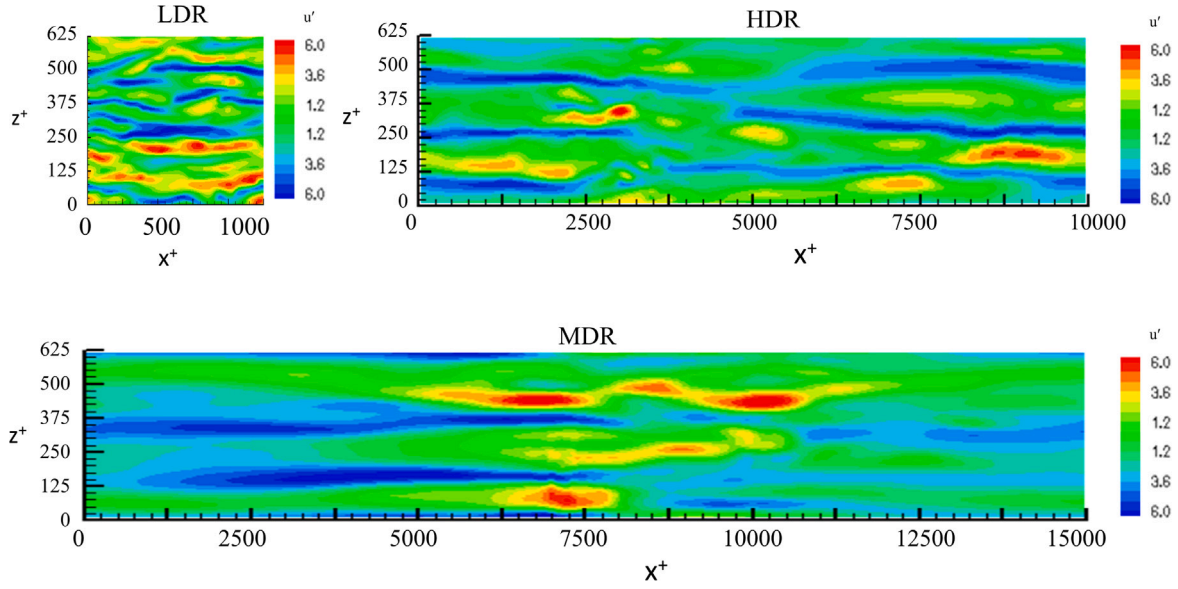

Fig. 9. Representative snapshots of velocity streaks in the $x-z$ plane at $y^+ \sim 15$ in the LDR, HDR, and MDR regimes. In highly drag reduced flows, *i.e.*, HDR and MDR regimes, highly organized low-speed streaks are observed. Accurately capturing these structures necessitates the use of very long domains, *i.e.*, $L_x^+ \geq 10{,}000$ in the HDR regime and $L_x^+ \geq 15{,}000$ in the MDR regime [118]. The dimensionless length in wall units is defined as $L^+ = LU_\tau/\nu$.

flows. Many different mechanisms for the occurrence of this intriguing phenomenon were proposed. These include: (1) the MDR profile is an edge solution of the Navier–Stokes equations with an effective viscosity profile beyond which no turbulent solution exists [128], (2) hibernating turbulence exists very near the boundary between laminar and turbulent flows [129], (3) MDR occurs when the quasi-streamwise vortices becomes on the order of the channel height [130], and (4) the ratio of the convective time scale associated with streamwise vorticity fluctuations to the vortex rotation time decreases with increasing DR, and the maximum drag reduction asymptote is reached when these two time scales become nearly equal. That is the energy extraction and release cycle gets interrupted. In turn, the flow state becomes weakly turbulent, in fact, laminar-like and eventually, the system transitions back to active turbulence and the stochastic cycle repeats [131]. Despite the fact that the mechanism postulated by Li, Sureshkumar, and Khomami [131] did not received much attention from the research community, it is entirely consistent with the newly proposed mechanisms for the occurrence of MDR as discussed below.

In the past decade, research focused on uncovering the origin of MDR has moved past the universality of the Virk asymptote mainly due the following reasons: (1) there is *no a priori* physical argument for a logarithmic relationship other than a simple analogy to the von

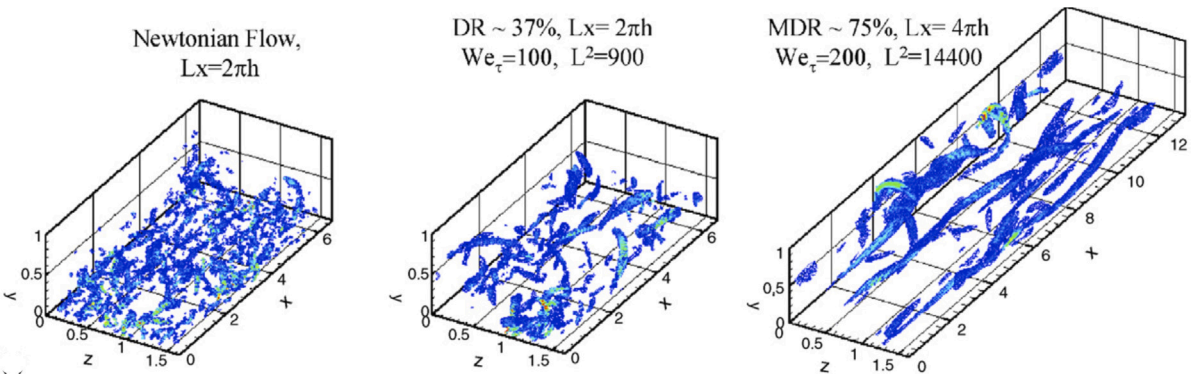

Fig. 10. Vortex structure at various %DR at $Re_\tau = 395$ [118].

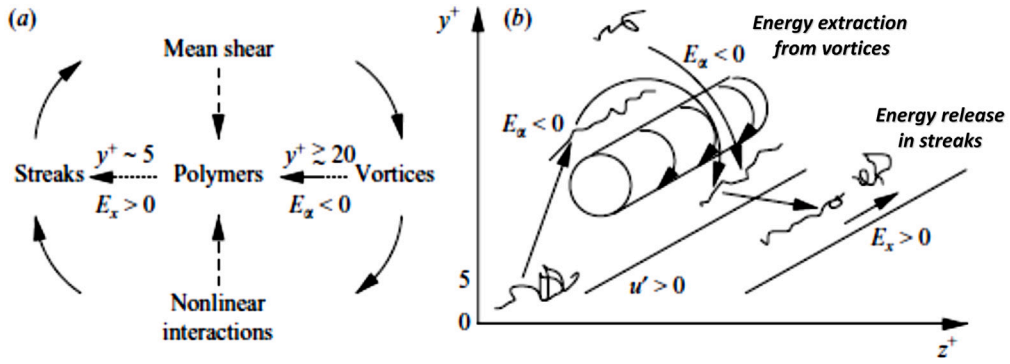

Fig. 11. (a) Cycle of wall turbulence regeneration with energy transfer from the polymers to the flow and vice versa, (b) Polymers extract energy from the flow as they are pulled around the near wall vortices either by upwash or downwash flows, hence, damping turbulence. In turn, polymers release energy back to the flow in the high-speed streaks thereby enhancing turbulence [117].

Kármán law, and (2) coefficients in the Virk asymptote are empirically determined from experimental data. In addition, recent experiments by Elbing *et al.* [132] and DNS and critical examination of existing data by White *et al.* [133] shows that a logarithmic relationship is probably inaccurate and the semi-log nature of the plot can be misleading, *i.e.*, non-logarithmic profiles cannot be clearly distinguished from logarithmic ones.

Motivated by these new observations, a flurry of studies on understanding the mechanism of the MDR began in early 2010s. These studies have discovered that in parallel shear flows, a full transition road map from inertial turbulence (IT) to a new turbulent-like regime dubbed elasto-inertial turbulence (EIT) exists [134–139]. Specifically, a reverse transition route from IT via a laminar base flow to EIT, is realized in pipe flows at a sub-critical Re of $O(10^3)$ [137,138], where upon enhancement of elastic forces either by increasing the polymer concentration and/or increasing Wi to $O(10)$ the flow first relaminarizes as the inertial quasi-streamwise vortices are gradually weakened and are finally eliminated [137–139]. This is reminiscent of the route proposed by Li, Sureshkumar, and Khomami in 2015 [131]. This relaminarized state exhibits drag reduction beyond the Maximum Drag Reduction (MDR) asymptote and subsequently undergoes a secondary instability, namely, elasto-inertial instability that results in dominant flow structure consisting of $2D$ sheets of highly stretched polymers in channel flows and streamwise elongated streaks in pipe flows [137–139]. An important advancement toward understanding the EIT dynamics has been achieved recently by Shekar et al. [140]. Specifically, they have shown that the trains of weak spanwise-oriented flow structures with inclined sheets of polymer stretch are related to a new viscoelastic nonlinear Tollmien–Schlichting attractor, that is nonlinearly sustained by viscoelastic stresses. Hence, it is not surprising that the EIT regime appears to have a physical origin that is similar to elastic turbulence as evidenced by the kinetic energy spectrum decay with scaling of −14/3, which is distinctly different from the Kolmogorov scaling of −5/3 for IT but close to the −3.5 scaling for ET [134–136,141,142].

3.2. Polymer induced drag modification in Taylor–Couette flow

In Section 2.2, it was shown the Oldroyd-B model has been successfully used to demonstrate that the Reynolds stresses are mainly responsible for stabilization (in the case of outer cylinder rotation) and destabilization (in the case of inner cylinder rotation) of the viscoelastic TC in the presence of fluid inertia. However, this model has not enjoyed wide spread use in investigating polymer induced phenomenon in turbulent TC flow due to the presence of elasticity-induced highly localized structures in the near wall regions that give rise to very strong elongational flows. The exception being a very few studies focused on the onset of elastic turbulence in *two-dimensional* TC flows. Chief among them is a recent study by Buel *et al.* [143], that demonstrates that beyond a critical Wi, an elastic instability causes a supercritical transition from the laminar Taylor–Couette flow to a turbulent flow. In addition, they demonstrate an increase in flow resistance and temporal power spectra of the velocity fluctuations that are reminiscent of elastic turbulence (see Section 2.3 for details).

Liu and Khomami [144] performed the first DNS of turbulent viscoelastic TC flow using the FENE-P model with $L^2 = 14400$ and $E = 0.02$ and demonstrated that upon addition of trace amounts of soluble high molecular weight macromolecules the Newtonian large-scale Taylor vortices are replaced by small-scale vortices in the inner and outer wall regions (see Fig. 12). In turn, it was shown that this flow transition and a commensurate drag enhancement (DE) of up to 62% are due to the occurrence of an inertio-elastic Görtler instability in the stationary outer wall region triggered by very large polymeric normal stresses.

The DNS of Liu and Khomami [88] in the viscoelastic TC flow for the range $0.2 \leq E \leq 5$ underscores the strong competition between fluid inertia and polymer induced elastic forces in the flow. Thus, a fundamental question arises, namely, how does the variation of inertial effects modify flow structures and turbulence characteristics as well as the flow-microstructure coupling in the inertio-elastic turbulent flow of viscoelastic TC flow where hoop stresses play a central role in driving flow transition and nonlinear dynamics?

Some progress toward answering the above-mentioned question has been made. Specifically, experimental observations of Lee et al. [145] indicate that polymer additives suppress the centrifugally-driven formation of Görtler vortices (GV) in $1500 < Re < 30000$. More recently, Latrache et al. [146] have identified two regimes of turbulence in the viscoelastic TC fows of shear-thinning PEO-alcohol–water solutions ($0.01 < E < 0.05$), namely, spatiotemporal intermittency and inertio-elastic turbulence. In addition, as described above, Liu & Khomami [144] have shown the occurrence of an inertio-elastic Görtler instability (IEGV) near the outer wall that leads to the breakdown of large scale Newtonian TV and a commensurate DE in the viscoelastic turbulent TC flow at $Re = 5000$ and $E = 0.02$. Moreover, the DE in viscoelastic turbulent TC flow shows a strong curvature dependence, namely, for a small radius ratio, $\xi = R_i/R_o$ the large-scale TV are destabilized by an elastic/inertio-elastic Görtler instability near the inner/outer wall; while for a large ξ, well-organized TV occupy the entire gap due to the stabilizing effects of elasticity [147]. Although, this curvature dependence can be rationalized in terms of the competition between elastic hoop stresses, fluid inertia and the important influence of polymer chain vortex interactions, the flow transition in the limit of zero curvature, namely, that of the span-wise-rotating plane-Couette flow with polymer additives is extremely interesting as the flow mainly consists of large scale roll-cells. Hence, one would expect that the polymer interactions with large scale roll cells would have the greatest influence on flow transition and drag properties. To this end, recent DNS studies of Zhu et al. [148] have demonstrated a reverse transition pathway from a Newtonian turbulent rotating plane-Couette flow to a fully re-laminarized DE viscoelastic flow consisting of large-scale and highly organized roll cells. Evidently, as Wi is increased small-scale vortices gradually weaken and are eventually eliminated. As foreshadowed above, the flow physics behind this intriguing flow transition is intimately related to the polymer chain interactions with vortices, which in fact, is very similar to that of polymer-induced transition toward MDR in unidirectional planar flows via the relaminarization route [135–140].

This finding plus a rigorous energy exchange analysis between turbulent motions, mean flow, and polymer chains demonstrates *the existence of a universal coupling dynamics between polymer chains and turbulent vortices* in wall-bounded viscoelastic flows. Evidently, realization of polymer induced DR or DE depends on the relative magnitude of DR realized via elimination of small-scale vortices to the DE that results from polymer chain interaction with large-scale roll cells and IEGV. This hypothesis is further substantiated by observation of a low degree of polymer induced DR, *i.e.* $\sim 35\%$ at $O(1)$ values of Wi, in the turbulent plane-Couette flow where small-scale vortices predominately occupy the near wall region, while the center of the channel is mainly populated by large scale roll cell like structures [149]. To this end, DNS of turbulent plane-Couette flow at high Wi is of great interest as it allows further examination of the universal polymer vortex interaction postulated above.

Motivated by the above-mentioned intriguing phenomena in the inertio-elastic TC flow, Liu, Khomami and co-workers [150] performed extensive DNS with the FENE-P model ($L = 100$) to examine the flow structure, spectral universality and the turbulence dynamics of this flow in the inertio-elastic regime. Specifically, a large radius ratio $\xi = R_i/R_o$=0.5, at five Re, ranging from 500 to 8000, corresponding to a range low to moderate values of E – 0.00375 ≤ E ≤ 0.06 – were considered. This comprehensive study has shown that as Re is increased, the turbulence dynamics can be conveniently subdivided into two distinct regimes: (1) a low $Re \leq 1000$ regime where the flow physics is essentially dominated by nonlinear elastic forces and the main contribution to transport and mixing of momentum, stress and energy comes from large-scale flow structures in the bulk region and the energy spectra decays with a −3.5 slope suggesting spectral universality of elasticity dominated turbulence, (2) a high $Re \geq 5000$ regime where inertial forces govern the flow physics and the flow dynamics is mainly controlled by small-scale flow structures in the near-wall region and as expected the energy spectra decays with a slope of −5/3 (see Fig. 13).

Table 1
Percent Drag reduction as a function of elasticity number. ($Wi = 30$, $L = 100$, $\xi = 0.5$, $\eta_s/\eta_T = \beta = 0.9$).

E	0.06	0.03	0.01	0.006	0.00375
%DE	33%	52%	54%	60%	43%

To understand the flow-microstructure coupling and the resulting flow dynamics modifications, Liu and Khomami and coworkers [88] carried out a detailed budget analysis of energy exchange between turbulent motions, mean flow and polymer chains. Specifically, examination of the mean kinetic energy (MKE) budget demonstrates that the polymer chains mainly absorb MKE and convert it to mean elastic potential energy through macromolecular extension driven by the mean flow. Also, examination of the total kinetic energy budget (TKE) budget shows that the polymer absorbs TKE from the fluctuating motions near the wall and then releases it to the near wall small-scale fluctuations to preserve the global dynamics. Furthermore, the Reynolds shear stress budget indicates that the elastic stress work has a negative contribution near the inner wall and slightly away from the outer wall; hence, it acts to suppress the production of turbulent shear stresses. However, in the bulk and in the vicinity of the outer-wall, elastic stress work has a positive contribution that facilitates the production of turbulent shear stresses. Evidently, increased fluid inertia hinders the generation of elastic stresses, leading to a monotonic depletion of the elastic-related nonlinear effects. To this end, a modest non-monotonic increase in DE is observed as Re is enhanced (see Table 1). As expected, %DE observed is consistent with earlier studies of Liu and Khomami [144] at $E \sim 0.02$. However, the non-monotonic increase in %DE might appear counter intuitive, since Song et al. [151] found that for most values of the radius ratio ξ elasticity stabilizes well-organized TV that occupy the entire gap. But, their study was performed at $E = 0.02$ and $\beta = 0.8$ as opposed to $\beta = 0.9$ in their more recent study. Hence, a direct comparison of the stabilizing effect of elasticity on the TV between these two studies cannot be conclusively performed. This clearly underscores that to fully understand the complex competition between elastic and inertial effects and thoroughly examine the *postulated universality of polymer vortex interactions*, a systematic study of drag modifications in the viscoelastic TC flow by variation of E and the gap width/curvature while keeping constant $\beta \geq 0.9$ and $L \geq 100$ is needed.

The elastically dominated turbulence (EDT) in TC flow displays principal differences with elasto-inertial turbulence in the channel and pipe flows due to the persistence of large-scale vortical structures *and* the curvilinear streamlines of the TC flow. Evidently, EDT is dominated by the *large-scale streamwise vortical structures* while EIT is sustained by trains of *spanwise-oriented flow structures* with inclined sheets of stretched polymer chains [140]. Despite these stark differences in the flow coherent structures, these two types of elastically dominated turbulent flows exhibit similarities in the generation of turbulence and Reynolds stresses. Very recently, Khalid et al. [152] have postulated that for highly elastic ultra-dilute polymer solutions, *a single linearly unstable branch may underlie transition to ET at zero Re, and to EIT at moderate Re,* implying the existence of continuous pathways connecting

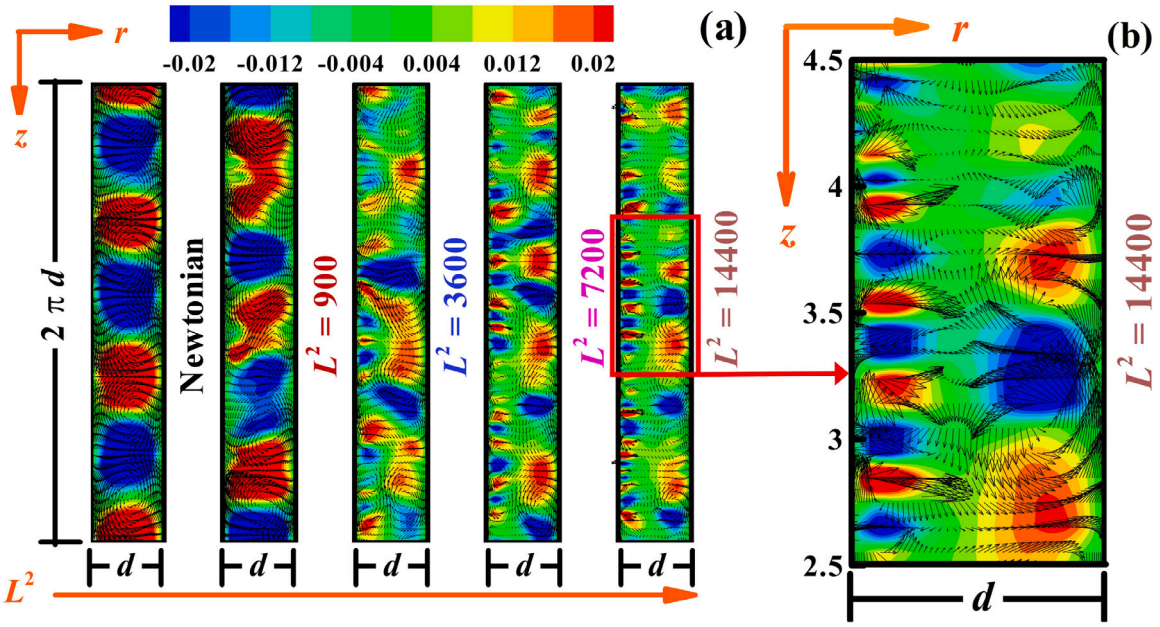

Fig. 12. (a) Time and θ-direction averaged vectors of radial (u_r) and axial (u_z) velocities and contour plots of u_r in the $r-z$ plane. (b) Magnified image of (a) for $L^2 = 14400$. The blue (dark) and red (light) contour regions correspond to radial inflow ($u_r < 0$) and outflow ($u_r > 0$), respectively.

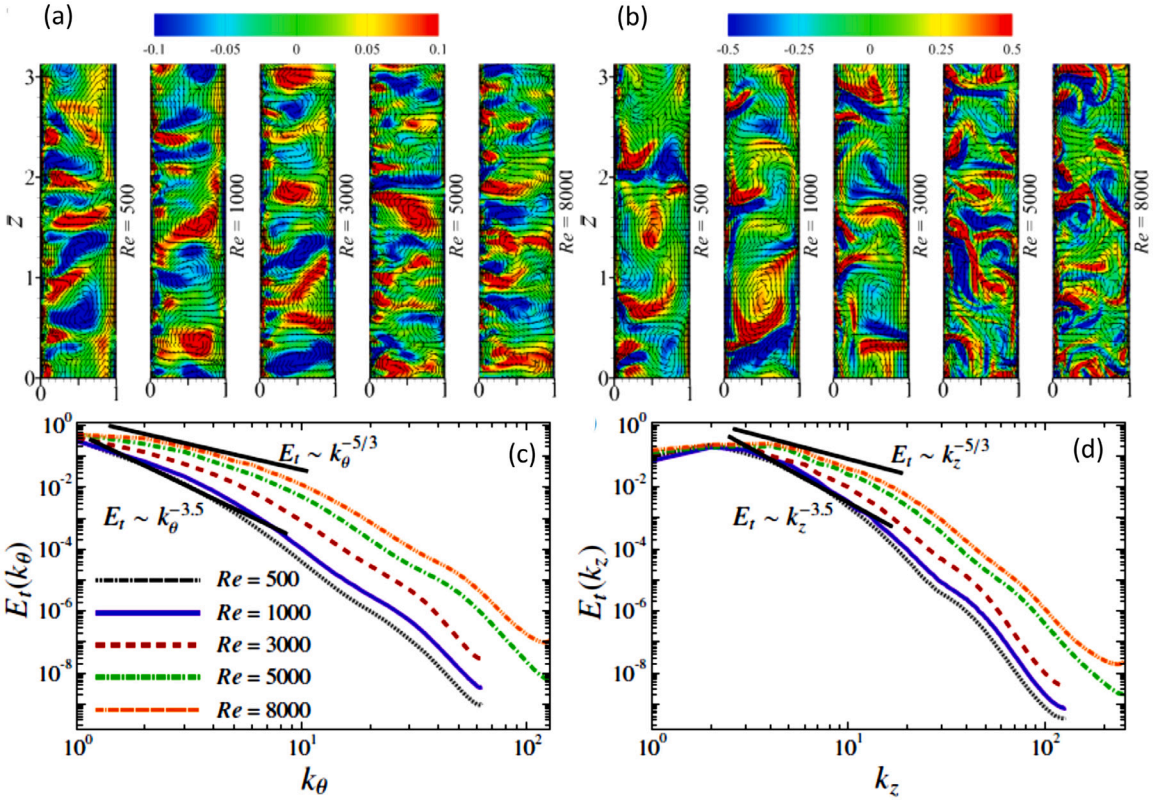

Fig. 13. (a) Time and θ-direction averaged vectors of radial ($\langle u_r \rangle_{\theta,t}$) and axial ($\langle u_z \rangle_{\theta,t}$) velocities and contour plots of stream-wise velocity ($\langle \omega_\theta \rangle_{\theta,t}$) in (r,z) plane. (b) Instantaneous vectors of radial (u_r) and axial (u_z) velocities and contour plots of u_r in the $r-z$ plane with $\theta = \pi/2$. (c)&(d) One-dimensional streamwise (c) and span-wise (d) spectra of the turbulent kinetic energy ($\langle \mathbf{u}'.\mathbf{u}' \rangle/2$) normalized by the stream-wise turbulent kinetic energy ($\langle u'_\theta u'_\theta \rangle/2$ sampled at the middle of the gap for various Re.

the turbulent states to each other. Although this postulate is intriguing, much more detailed analysis is required before conclusive statements regarding *the universality of key features of the flow and energy spectra of elastically driven turbulence* in either the absence or presence of moderate inertia can be made. To this end, Liu, Khomami and co-workers have very recently carried out extensive DNS in viscoelastic TC to examine the transition from inertial to elasticity-dominated turbulence including the intriguing purely elastic turbulent flow state [151].

4. Oldroyd-B fluid in understanding particle flows and motions in elastic fluids

4.1. Uniform flow past fixed particles and sedimentation

One of the most celebrated "failures" of the Oldroyd-B model is associated with the uniform flow past particles at vanishingly small Reynolds number, and, in retrospect, this has been critical to creating guiding principles for the model's application to new problems. It is now a matter of historical fact, that for uniform flow past rigid, fixed bodies (most notably spheres and cylinders) at low Reynolds number, the structure of the flow is such that there exist wake regions of locally extensional flow where the Oldroyd-B model is inappropriate to describe the flow of dilute polymer solutions. This follows since the model demonstrates a critical value of distance downstream of the rear stagnation point where the local value of the Deborah number (i.e. the relaxation time times the local extension rate) $De \geq 0.5$ and the accumulated Hencky strain is large such that a "stress singularity" is approached. (Note in this context that the flow Deborah number is typically defined $De = \frac{\lambda U}{R}$, where U is the constant flow velocity far upstream and R is a characteristic length scale for the particle.)The existence of a critical value of the Deborah number was surmised in an early paper by Rallison and Hinch [153]. In a paper near that time, Chilcott and Rallison [154] demonstrated that numerical issues in calculating the Oldroyd-B flows past spheres or cylinders beyond a critical value of the flow Deborah number (as experienced by themselves and other authors), could be alleviated by the introduction of FENE type models (though in this instance, they used the so called FENE-CR model [154] which is not one the three discussed in Section 1 of this article). This issue was thoroughly examined by Bajaj et al. 2007 [155], where they demonstrated quite convincingly that the polymer stress becomes singular for the Oldroyd-B fluid in the wake of a circular cylinder past a critical value of the flow Deborah number (cf. Fig. 14). Note the critical value of the flow Deborah number was a function of the polymer concentration parameter β and actually decreased as more polymer was introduced. One of the key tools that they used to demonstrate the singularity was configuration solutions in the so-called "ultra-dilute" limit which is the limit $\beta \rightarrow 1$ where the kinematics are Newtonian and one simply integrates the conformation equations along streamlines (this is the *method of characteristics* applied to the OB fluid model). Referring to Fig. 14, we see that the singularity is removed for the FENE-P model, as the polymer spring force stiffens and the stretch approaches its maximum extensibility. A similar study was accomplished by Abedijaberi and Khomami [156] fror the analog problem of single particle sedimentation, demonstrating converged numerical solutions could be found for flow past a sphere using the FENE-P model, but the problem became increasingly difficult to solve (and the stress grew in the wake behind the sphere) as the parameter L increased. This problem – i.e. that there can be points in a flow which are extensional in character and in which the Oldroyd-B model can exhibit unbound conformation stretch and hence stress growth past a certain critical Deborah number – is referred to as the "High Weissenberg Number Problem" (HWNP). This problem is exacerbated – meaning the critical value of the flow Weissenberg or Deborah number is lower – for other common particulate problems, including flow past a bubble (i.e. stress free interface [154]) and the flow created by an active "squirmer" particle swimming in an elastic fluid [157] . A somewhat more generic definition of the HWNP is that there can be thin regions of high polymer stretch and thus stretch gradient for flows at $Deborah$ or $Weissenberg$ number which are $O(1)$ and these regions can make numerical methods non-convergent and/or inaccurate. *Note that these two statements of the HWNP are not the same.* There can be thin regions of high polymer stress and thus high stress gradients even with the FENE-P models and these can be very difficult to resolve, even if the stress in the Oldroyd-B model is not singular at a critical point or points in the flow. After recognizing this problem in the Oldroyd-B model, most researchers use numerical methods for flows involving particles which employ the FENE-P model (or, alternatively, the Giesekus model) which we know remove the possibility of a stress singularity. More recently use of the Oldroyd-B model for particle flows has had something of a rebirth, primarily because it has been found that the wake structure for flow past a rigid particle is not similar for other particle flows – e.g. uniform flow past a sphere *combined* with shear flow. In these cases, we can safely return to the Oldroyd-B model, and it has again been used to learn a great deal about particle motions in elastic fluids.

Beyond the HWNP, another "failing" of the OB fluid in the solution of uniform flow past a rigid particle, is that for values of the Deborah number below the critical value, the drag on the sphere (or cylinder per unit length) *decreases* whereas experiments show a monotonic drag increase. Even after "regularizing" the problem via the FENE-P, this reduction in drag at small values of De remains but is followed by an increase in drag at higher values of De. Yang and Khomami [158] as well as Abedijaberi and Khomami [156] completed exhaustive numerical studies of this problem and demonstrated that experimental values of the drag coefficient could be well approximated, but only with a multi-mode FENE model *without* pre-averaging. Thus the nonlinear coupling of multi-modes present in a real polymer molecule and absent from pre-averaged closed constitutive equations is important to correctly calculate the dissipation and drag in flow past fixed objects.

4.2. Shear flow of freely suspended cylinders/spheres in suspension

One can argue that the three most fundamental flows in the suspension mechanics of Newtonian fluids are (a) flow past a fixed particle, (b) motion of a particle under constant body force, and (c) motion of a freely suspended particle in a shear (or general linear) flow. Each of these is associated with a different property of a suspension: (a) the effective permeability of a fixed medium, (b) the average "slip" or separation velocity under applied body force and (c) the effective rheology of a suspension of freely suspended particles. Batchelor, his students and co-workers [7,160], in their seminal body of work, demonstrated the foundational principles of low Reynolds number suspension mechanics, examining these three flows. As described above, flows (a) and (b) have been shown to demonstrate the HWNP for the Oldroyd B fluid, and, as a result progress in understanding the physics of these two flows was slow. All computational solutions generally use FENE-P or Giesekus models if a closed form constitutive equation is chosen. However, the first numerical solutions for single freely suspended particles in an elastic linear flow (c), were for the Oldroyd-B fluid and focused on cylinders in simple shear flow [see Hwang et al. [161]]. These two dimensional solutions were accomplished up to values of the shear Weissenberg number of unity with apparently no convergence problems. Note that, as reported later for shear flow past a sphere in Fig. 15, the wake structure is entirely different in this flow relative to uniform flow past a particle. Because the sphere/cylinder rotates in the shear flow (to satisfy the no torque condition) there are no stagnation points near the body. Indeed the flow is divided via a separatrix into a closed streamline region near the particle, where, a polymer undergoes periodic sampling of flow which is alternatively uniaxial and biaxial extension. A polymer in such a flow never experiences large Hencky strain in any of the extensional regions of the flow, since the rotation rate of the particle is of the size of the local vorticity. The first groups to accurately calculate shear flow past a sphere via the Oldroyd-B model were D'Avino et al. [162], Yang et al. [163], Einarsson et al. [164], and Koch et al. [165]. D'Avino et al. [162], originally completed the problem for the Maxwell fluid (i.e. $\beta = 0$ in the Oldroyd-B) and focused on the *slowing* of the rotation rate of the sphere, below the Newtonian value (the latter is classically one half the local fluid vorticity) created by elasticity. Yang et al. [163] completed the problem for finite polymer concentration ($\beta \leq 1$) via a finite volume scheme up to values of the shear flow Weissenberg number, $Wi \leq 0.5$. They also did the so called "ultra-dilute" problem

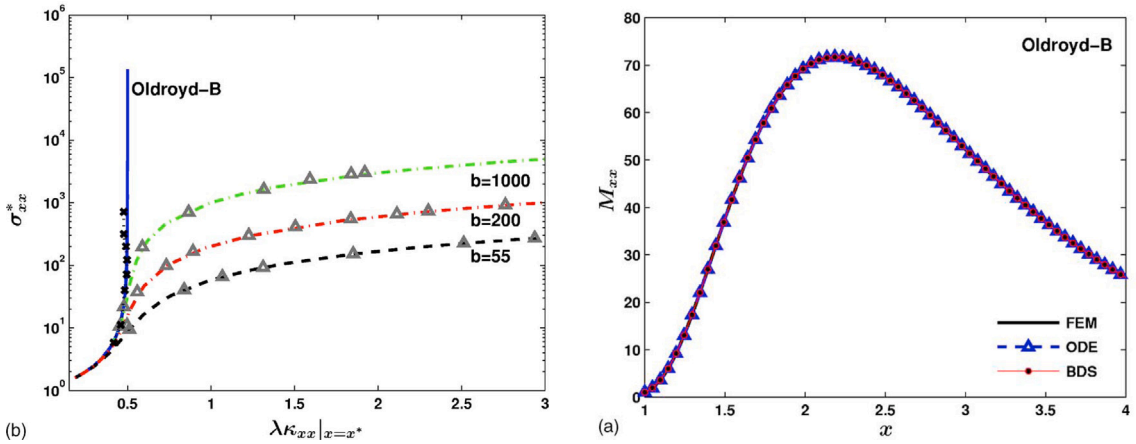

Fig. 14. LEFT– Simulated values of the polymer stress in the wake behind a cylinder for the Oldroyd B Model and various FENE-P models as a function of the local Deboarah number at the stress/stretch maximum. The flow kinematics are such that the solution is "ultra-dilute" (i.e. $\beta = 1$) and the flow is therefore Newtonian. Again $b = 3L^2/(N_k b_k^2)$ in the notation of the present article; RIGHT – Polymer conformation dyad dimensionless $< R_1^2 >$ (here denoted by M_{xx}) as a function of distance in the cylinder wake at a flow Deborah number of 0.8.[155].

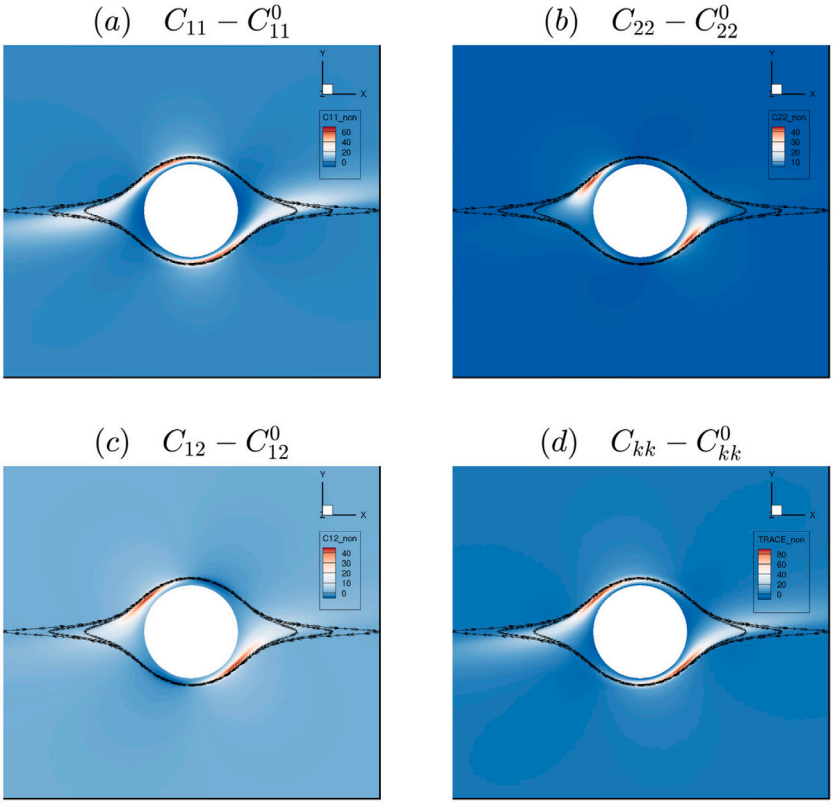

Fig. 15. Simulated components of the polymer conformation dyad $C_{ij} = \overline{< R_i R_j >}$ (minus that of the fluid in the absence of the particle) for the Oldroyd-B model for shear flow past a sphere. The Weissenberg number is 2 and the calculations are completed in the limit as $\beta \to 1$, i.e. the flow kinematics are Newtonian. The separatrix and regions of recirculation are clearly shown.
Source: Adapted from Fig. 9 in [159].

in a similar fashion to Bajaj et al. [155] where the flow is Newtonian, and the polymer conformation tensor is solved in the Newtonian flow field (cf. Fig. 15 for the ultra-dilute stress contours). Koch et al. [165] were the first to demonstrate via the Oldroyd-B model and using the method of characteristics in the ultra-dilute limit, that a polymer along any of the streamlines of the Newtonian flow, does not experience a large Hencky strain at any point. No approach to a singular stress was demonstrated even for values of $Wi \sim O(1)$. Einarsson et al. [164] used the Oldroyd-B model calculations to verify their retarded motion expansion ($Wi \ll 1$) of the same problem. Yang and Shaqfeh [159] later revisited this problem and obtained convergent results for the OB fluid for all polymer concentrations up to Weissenberg numbers $Wi \leq 5$. Note that these authors also completed a comparison of the shear flow problem in the three models: Oldroyd-B, Giesekus, and FENE-P. These authors came to two important conclusions: (a) that while there was no indication of a stress singularity, the regions of high polymer stress were confined to increasingly thinner regions with increasing Weissenberg number and thus the stress gradients became increasingly difficult to resolve (i.e. the more general statement of the HWNP was true for the shear flow problem), and (b) the magnitude of the polymer

stress and stress gradients were significantly greater for the Oldroyd B model at values of $Wi \sim O(1)$.

The importance all the publications mentioned in the paragraph above, is that with the numerical solution in hand for the stress field, the average rheological response of an elastic fluid with the dilute addition of spherical particles could be theoretically predicted and compared to experiments. There has been a recent review paper [166] which focuses on the various measurements (and comparison to predictions) of the rheological properties of non-colloidal suspensions in a variety of non-Newtonian matrices including elastic fluids. We will attempt not to repeat much of the work described in that review. Instead, for the purposes of the present article, we will focus on modeling and how it relates to the OB fluid. Thus, As originally discussed by Koch and Subramanian [167] and Rallison [168] regarding the second order fluid, for nonlinear fluid constitutive equations, the contributions to the change in rheology of a suspension by the particles falls into two categories: (a) the stresslet contribution, that results from the particles themselves having a different constitutive equation than the fluid and (b) the average change in the local stress in the suspending elastic fluid. The latter contribution is termed the *particle induced fluid stress* (PIFS) [159,163]. It averages to zero in Newtonian fluids because of the linear constitutive equation, but produces a nonzero average for elastic fluids. All researchers in theoretical or computational modeling have found that particles in an Oldroyd B fluid produce a "thickening" of both the shear viscosity and primary normal stress coefficient even for single particles (meaning without particle–particle hydrodynamic interactions) (cf. Fig. 16). This was found even in the simulations by Hwang et al. for cylinders [161], where the partitioning of the stress increase into stresslet and PIFS was not established. While the stresslet actually decreases with increasing Wi the PIFS is found to increase, and the latter overwhelms the stresslet to produce a net increase in these two average material properties– the viscosity and primary normal stress coefficient. Such a thickening is seen in both properties in experiments, even at particle concentrations as low as 2.5% [169,170] (cf. Fig. 16). These findings can be viewed as another modern success of the Oldroyd-B model.

Note that generally the predictions of the aforementioned thickening of the rheological properties within single particle theories/computations are not quantitative in comparison to experiments [166]. Simulations of single particles in the shear flow of an Oldroyd B fluid generally under-predict the experimentally measured per particle extra stress even if the fluid parameters are carefully matched [163,169]. Note that as of the writing of this manuscript, four research groups [15, 169–171] have now examined fully three dimensional, multi-particle simulations of spheres in an Oldroyd-B fluid to examine concentration effects on the material properties of non-Brownian suspensions. Three of these groups [15,170,171] claim quantitative agreement with experimental data (and note different experiments with different elastic fluids !) up to $We \leq 3$ using a multi-mode Oldroyd-B model. The tentative finding is that hydrodynamic interactions affect the suspension properties above volume fractions in the range $0.025 \leq \phi \leq 0.1$ but only through increasing the stresslet at a given Weissenberg number (i.e. the PIFS seems to be a local property of the polymer fluid interactions) [15] . These conclusions have been reached over a very limited range of simulation conditions with comparison to existing experiments and much more needs to be done to examine the rheology over a broader range of polymer concentration, particle concentration, and Weissenberg number. For example, it has recently been reported via numerical simulation (and demonstrated in previous experiments) that freely suspended spheres in a shear flow can form "chains" in elastic fluids [172]. However the rheological properties necessary for chaining is still a subject of debate and appears to require normal stresses and significant "shear thinning" [172]. Such structures could have a profound effect on the rheology of suspensions, but no chaining apparently occurs in Boger fluids or was reported in the experiments/multi-particle simulations discussed above [169]. Moreover, if the flow is changed to *extensional flow* then the existing studies with the Oldroyd-B [164,173] predict "thickening" and then "thinning" as a function of *Hencky strain*. A review of the experimental data regarding extensional rheological measurements in particle suspensions within elastic fluids suggests that no clear trends or general understanding are available [166]. The Oldroyd-B fluid has and will have a big role to play in these studies as they progress, if only to contrast the behavior found in other, more complex, elastic fluids.

4.3. Particle migration in shear flows of viscoelastic fluids

The cross stream migration of freely suspended particles (*i.e.* no external applied forces or torques) in viscoelastic fluids is now a subject which is very mature and dates from the original experimental work of Karnis and Mason,1966, [174] who examined migration in scenarios where the shear rate varied across streamlines. Indeed, the first theoretical predictions of the migration velocity were made using the second order fluid and were established by perturbations in small Weissenberg number [174]. Migration was found to be generally toward regions of low(er) shear and created by normal stress imbalances on either side of the particle, in a flow in which the shear rate varies. However, at finite values of the Weissenberg number, employing a very broad and complete set of numerical simulations, Li et al. [175] demonstrated that this conclusion was true for the Oldroyd-B fluid, but if the shear thinning was significant enough, migration to the walls could occur, with even intermediate positions (between wall and centerline) becoming attractors. This general topic is now seeing renewed interest because of its use in microfluidic applications [176]. Apparently, the first numerical simulation of this phenomenon was for pressure driven flow in a channel past a cylinder where the cross stream migration force/velocity was determined using the Oldroyd-B fluid [177]. Later, calculations for spheres were accomplished using the ALE technique employing the Giesekus constitutive equation [178] and an "immersed force" technique [175] for Oldroyd-B and Giesekus constitutive equations. The recent review paper [174] is quite complete on the subject. Perhaps one of the most interesting conclusions from this body of work is that migration can occur with walls even in simple shear flow (*i.e.* constant shear rate) induced by the walls. This was predicted and analyzed by using the Giesekus constitutive equation [179]. In this case, proximity to the walls induces a "slip" velocity between the particle and fluid, which in turn creates a normal stress imbalance across the particle and an elastic "lift" force — and thus "drift" for a particle that is freely suspended. Such a "viscoelastic lift" can be engendered in alternative ways as discussed in the next section.

4.4. Combining shear flow and a particle body force – Particle migration, lift and enhanced drag

Recently, researchers have shown quite clearly in experiments, that if one applies a body force to a particle while in a shear flow, the nonlinear coupling of the two in an elastic fluid can create interesting new phenomena [176,180–182]. The most notable of these is that mobility of the particle can be changed very significantly, and in general becomes anisotropic, depending on the principal axes of the shear flow [183] – even if the shear rate is constant and the flow is unbound, unlike the situations in the previous subsection. Thus for example, particle migration across streamlines can be engendered even if the body force is applied in the direction of the shear flow – or, in other words – there is a viscoelastic lift force, that, if not balanced by the applied force results in viscoelastic drift across streamlines. [184]. As another example, the drag on a particle in the direction of the body force can be greatly exacerbated via the shear flow in an elastic fluid [180,181,185]. One might think that, problems of this kind, are not amenable to analysis via the Oldroyd-B fluid because of the severe HWNP which exists in the case of the applied body force alone —

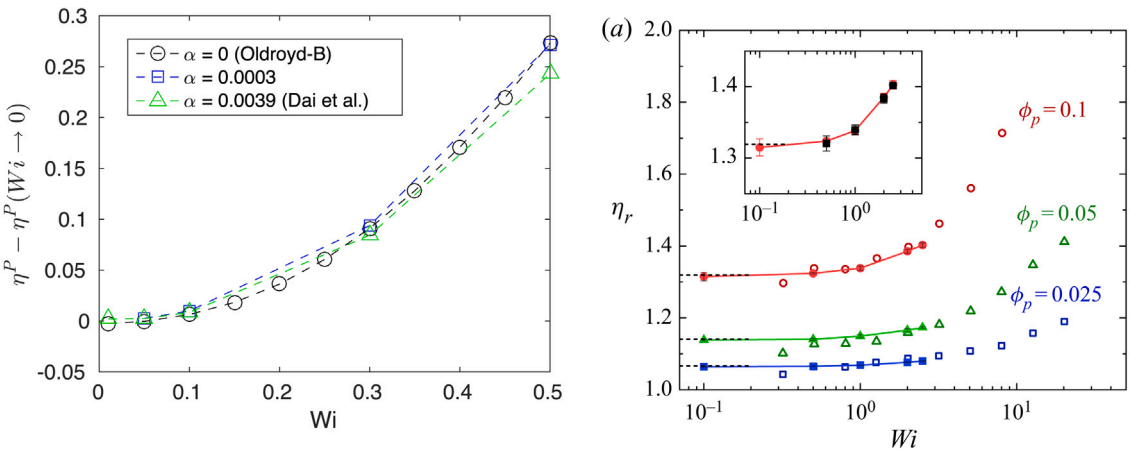

Fig. 16. LEFT — Simulated values of the "extra viscosity" for a single sphere as a function of Weissenberg number in the limit of zero polymer concentration (i.e. Newtonian kinematics) for the Oldroyd-B and Giesekus models [163]. RIGHT — Comparison of the multiparticle simulations using the Oldroyd-B Model and experimental data at 3 particle volume fractions [170].

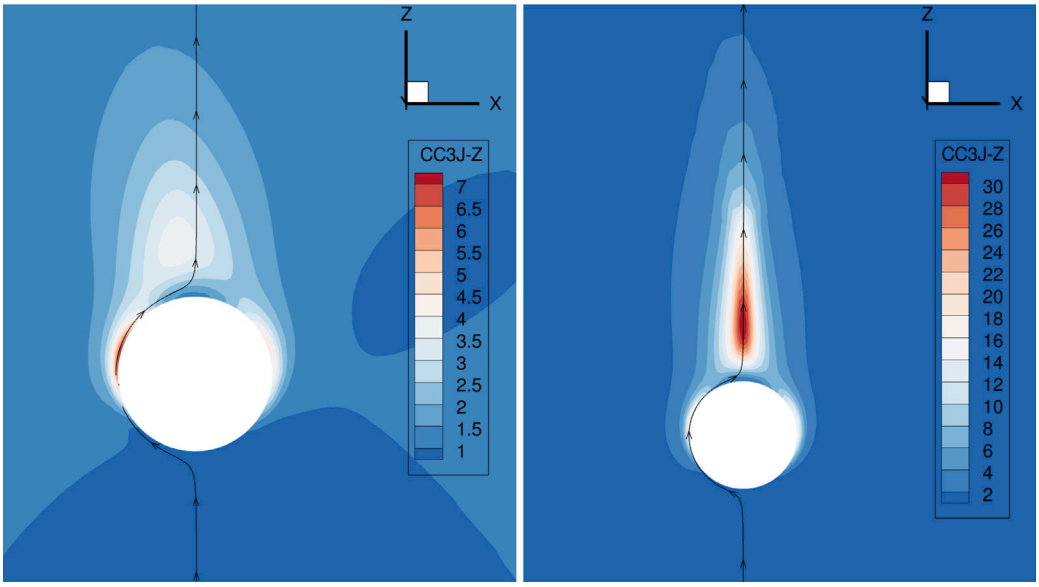

Fig. 17. LEFT — Simulations of a sphere settling in the Oldroyd B fluid in the -z direction under simple shear with the flow-gradient plane being z-x. The shear Weissenberg number is $Wi = 0.1$ and the flow Deborah number $De = 1$. The Deborah number, De, is defined as $De = \lambda U/R$ where U is the slip velocity between the particle and the fluid velocity at its center and R is the sphere radius. Note the increased polymer stress on the left of the sphere which has a higher velocity relative to the fluid than the right. RIGHT — Same simulations except $Wi = 0.1$, $De = 2$. A substantial stress wake does not form until $De \geq 2$ [182].

except of course unless perturbation theory is applied at low values of the Weissenberg number and Deborah number [181]. However, again, with the addition of a shear flow *and the condition that the particle is torque free*, the rotation of the particle changes the wake structure around the particle and alleviates all stagnation points from the surface. Thus it would appear that, for a given shear Weissenberg number, the value of the Deborah number based on the motion of the particle under the applied body force at which the HWNP for the Oldroyd-B fluid occurs can be significantly increased (cf Fig. 17). *In this discussion and that which follows, the Deborah number, De, is defined as* $De = \lambda U/R$ *where* U *is the slip velocity between the particle and the fluid velocity at its center and* R *is the sphere radius.* Moreover, algorithm development of viscoelastic flow solvers has recently focused on particle resolved calculations of suspension flows and the Oldroyd-B model has played a prominent role in this development [169,186,187].

The effects of the coupling of body force and shear flow was originally focused on the increase in the resistance (decrease in mobility) of spheres sedimenting in the vorticity direction of a simple shear flow as measured in the seminal Taylor–Couette cell experiments by Gheissary and Van Den Brule [180] There are now measurements of a reduction by a factor of 5 in sedimentation speed for spheres falling along the vorticity axis in viscoelastic fluids [185]. The mechanisms of this mobility reduction were elucidated first via perturbation theory for small shear Weissenberg number and sedimentation Deborah number employing the Oldroyd-B fluid [181]. This is again a modern triumph of the Oldroyd-B model. Later large scale numerical simulations verified this perturbation theory, and demonstrated that wall effects could be important, and particle interactions at finite concentration amplified the effect [185,188–190]. These numerical results generally employed the FENE-P or Giesekus fluid rheology, but were shown to agree with the perturbation of the Oldroyd-B fluid for Weissenberg numbers less than about 0.6 [188].

Even more dramatic than the reduction in particle mobility, are the drift velocities across streamlines that are produced by the coupling between applied body forces and fluid shear in viscoelastic fluids. For

example, these have been successfully used to "tunably" focus particles in microchannels [176]. Such migration can be created through combined electrophoresis and pressure driven flow [191,192]. Recently this particular application has been examined theoretically using perturbation theory and the second order fluid model [192,193]

Finally, suspensions of particles settling or rising (under a gravitational body force for example) in viscoelastic fluids are apparently almost universally unstable to concentration fluctuations — meaning they form clusters or streamers even though there are no apparent attractive forces between the particles [194,195]. The explanation for this latter phenomenon is apparently again, drift across streamlines in a shear flow created by a concentration fluctuation [182,190,196]. The Oldroyd-B fluid has played a role in this understanding. For example, Zhang et al. [182] did a broad examination of the lift and drag on rigid spheres and spheres which were shear stress free at their surface (e.g. undeformed bubbles) in an Oldroyd-B fluid under shear with a constant particle "slip" velocity relative to the local fluid velocity (driven for example, by an applied body force). The authors considered "slip" along the vorticity, gradient and flow axis for the rigid particle. Generally, values of $\beta = 0.3$ and 0.9 where considered along with the pair of condition ranges, (a) $Wi = 0.1, 0 \leq De \leq 2.5$ and (b) $De = 0.1, 0 \leq Wi \leq 3$. It was generically found that the force on the particle in the direction of the slip *increased* over the Newtonian value for all directions of slip and values of De. The largest increase in force (drag) occurred for slip along the gradient direction and the smallest increase was for slip along the shear flow direction. The force increased with Wi although it began to plateau for $Wi \geq 1$ and was relatively insensitive to De. For a bubble, the drag also increased with shear and was consistent with Tiefenbruck et al. [197,198] calculations for a third order fluid. In terms of the lift force, the most notable finding was that for rigid spheres and for spheres with a perfect slip boundary condition (i.e. a model for an undeformed bubble), the lift force drove particles toward the direction where the fluid flow increased *in the direction of the slip velocity*. This is consistent with the perturbation analysis of Einarsson et al. [183] and is the direction which implies concentration instability. This supports the notion that concentration instabilities in these systems under buoyancy (for example) are driven by lateral drift associated with concentration driven, shear flow fluctuations. Such a conclusion would be quite important as it provides a framework to continue our understanding of particle interactions in elastic fluids as discussed elsewhere [199] and serves to provide an understanding of bubble clustering in polymer solutions [200].

5. Summary and conclusion

We conclude by noting that Oldroyd's seminal 1950 paper [1] continues to have a vital life in the rheological community for a number of reasons. First, even though the model was developed originally as a study in viscoelastic fluid mechanics, its connection to the kinetic theory of polymer solutions gives it a direct physical connection to polymer solution dynamics. Moreover the model, in at least its multimode form, can reproduce the linear and nonlinear shear rheology of Boger fluids. In terms of the single mode formula, the constitutive equation is closed and the stress depends on a single dyad conformation tensor. Thus 6 equations are typically solved in addition to Cauchy's equations of motion, and this is now relatively easy with modern computing power. It follows that for shear flows, even time dependent shear flows, it is a starting point of choice. The difficult issue with the OB fluid is that it does present a singularity in extensional flow, and thus, when calculating or trying to understand complex mixed flows (i.e. those which have regions of extensional character) researchers often choose the FENE-P or Giesekus constitutive equations to avoid the High Weissenberg Number Problem. However, the value of the Oldroyd-B fluid, even if it is examined *after FENE-P or Giesekus calculations*, has been demonstrated time and time again — in particle flows, elastic instabilities and even in turbulent drag modification. It is perilous for a student of complex fluids to ignore analysis based on the Oldroyd-B fluid in any given elastic flow problem.

Declaration of competing interest

The authors declare that they have no known competing financial interests or personal relationships that could have appeared to influence the work reported in this paper.

Acknowledgments

ESGS would like to acknowledge the support by the National Science Foundation, United States under Grant No. CBET-1803765 for the work presented in Section 4 of this manuscript. The computations in Section 4 were performed on the Shepard and Yellowstone cluster at the Stanford HPC Center, supported through awards from the National Science Foundation, United States, DOD HPCMP, United States, and Office of Naval Research, United States. This work also used the Extreme Science and Engineering Discovery Environment (XSEDE), United States cluster Comet to perform simulations through allocation Grant No. MCB190002. We also acknowledge Anni Zhang for producing Fig. 17 from unpublished data associated with publication [182]. BK would like to acknowledge the support provided by the National Science Foundation, United States under award CBET-1602890 for the work presented in Section 3 of this manuscript. The computations performed in Section 3 is part of the Frontera computing project at the Texas Advanced Computing Center. Frontera is made possible by National Science Foundation, United States award OAC-1818253.

References

[1] J. Oldroyd, On the formulation of rheological equations of state, Proc. R. Soc. Lond. A 200 (1950) 523–541.
[2] D. Boger, A highly elastic constant-viscosity fluid, J. Non-Newton. Fluid Mech. 3 (1978) 87–91.
[3] R.G. Larson, Constitutive Equations for Polymer Melts and Solutions: Butterworths Series in Chemical Engineering, Butterworth-Heinemann, 2013.
[4] W. Kuhn, F. Grun, Relationships between elastic constants and stretching double refraction of highly elastic substances, Kolloid Z. 101 (1942) 248–271.
[5] F. Latinwo, C.M. Schroeder, Model systems for single molecule polymer dynamics, Soft Matter 7 (2011) 7907–7913, http://dx.doi.org/10.1039/C1SM05298E.
[6] H. Kramers, The viscosity of macromolecules in a streaming fluid, Physica 11 (1) (1944) 1–9.
[7] G. Batchelor, The stress system in a suspension of force-free particles, J. Fluid Mech. 41 (3) (1970) 545–570.
[8] C.M. Schroeder, R.E. Teixeira, E.S. Shaqfeh, S. Chu, Dynamics of DNA in the flow-gradient plane of steady shear flow: Observations and simulations, Macromolecules 38 (5) (2005) 1967–1978.
[9] A. Erdélyi, Asymptotic Expansions, no. 3, Courier Corporation, 1956.
[10] E. Hinch, Perturbation methods, 1991.
[11] P.E. Rouse Jr., A theory of the linear viscoelastic properties of dilute solutions of coiling polymers, J. Chem. Phys. 21 (7) (1953) 1272–1280.
[12] B.H. Zimm, Dynamics of polymer molecules in dilute solution: viscoelasticity, flow birefringence and dielectric loss, J. Chem. Phys. 24 (2) (1956) 269–278.
[13] D.F. James, Boger fluids, Annu. Rev. Fluid Mech. 41 (2009) 129–142.
[14] I. Garduño, H. Tamaddon-Jahromi, M. Webster, The falling sphere problem and capturing enhanced drag with boger fluids, J. Non-Newton. Fluid Mech. 231 (2016) 26–48.
[15] A. Jain, E.S. Shaqfeh, Transient and steady shear rheology of particle-laden viscoelastic suspensions, J. Rheol. 65 (6) (2021) 1269–1295.
[16] T. Sridhar, An overview of the project M1, J. Non-Newton. Fluid Mech. 35 (2–3) (1990) 85–92.
[17] R.G. Larson, The Structure and Rheology of Complex Fluids, vol. 150, Oxford university press New York, 1999.
[18] T.T. Perkins, D.E. Smith, S. Chu, Single polymer dynamics in an elongational flow, Science 276 (5321) (1997) 2016–2021.
[19] C.M. Schroeder, E.S. Shaqfeh, S. Chu, Effect of hydrodynamic interactions on DNA dynamics in extensional flow: Simulation and single molecule experiment, Macromolecules 37 (24) (2004) 9242–9256.
[20] H.R. Warner Jr., Kinetic theory and rheology of dilute suspensions of finitely extendible dumbbells, Ind. Eng. Chem. Fundam. 11 (3) (1972) 379–387.
[21] A. Cohen, A Padé approximant to the inverse Langevin function, Rheol. Acta 30 (3) (1991) 270–273.

[22] J.F. Marko, E.D. Siggia, Stretching dna, Macromolecules 28 (26) (1995) 8759–8770.

[23] R. Keunings, On the Peterlin approximation for finitely extensible dumbbells, J. Non-Newton. Fluid Mech. 68 (1) (1997) 85–100.

[24] G. Lielens, P. Halin, I. Jaumain, R. Keunings, V. Legat, New closure approximations for the kinetic theory of finitely extensible dumbbells, J. Non-Newton. Fluid Mech. 76 (1–3) (1998) 249–279.

[25] L.E. Wedgewood, D.N. Ostrov, R.B. Bird, A finitely extensible bead-spring chain model for dilute polymer solutions, J. Non-Newton. Fluid Mech. 40 (1) (1991) 119–139.

[26] H. Giesekus, A simple constitutive equation for polymer fluids based on the concept of deformation-dependent tensorial mobility, J. Non-Newton. Fluid Mech. 11 (1–2) (1982) 69–109.

[27] P.S. Doyle, E.S. Shaqfeh, Dynamic simulation of freely-draining, flexible bead-rod chains: Start-up of extensional and shear flow, J. Non-Newton. Fluid Mech. 76 (1–3) (1998) 43–78.

[28] S.H. Spiegelberg, G.H. McKinley, Stress relaxation and elastic decohesion of viscoelastic polymer solutions in extensional flow, J. Non-Newton. Fluid Mech. 67 (1996) 49–76.

[29] G.H. McKinley, T. Sridhar, Filament-stretching rheometry of complex fluids, Annu. Rev. Fluid Mech. 34 (1) (2002) 375–415.

[30] L. Li, R.G. Larson, T. Sridhar, Brownian dynamics simulations of dilute polystyrene solutions, J. Rheol. 44 (2) (2000) 291–322.

[31] A. Saadat, B. Khomami, Molecular based prediction of the extensional rheology of high molecular weight polystyrene dilute solutions: A hi-fidelity Brownian dynamics approach, J. Rheol. 59 (6) (2015) 1507–1525.

[32] G. Fuller, L. Leal, The effects of conformation-dependent friction and internal viscosity on the dynamics of the nonlinear dumbbell model for a dilute polymer solution, J. Non-Newton. Fluid Mech. 8 (3–4) (1981) 271–310.

[33] V.A. Beck, E.S. Shaqfeh, Ergodicity-breaking and the unraveling dynamics of a polymer in linear and nonlinear extensional flows, J. Rheol. 51 (3) (2007) 561–574.

[34] E.S. Shaqfeh, Purely elastic instabilities in viscometric flows, Annu. Rev. Fluid Mech. 28 (1) (1996) 129–185.

[35] B.M. Baumert, S.J. Muller, Flow visualization of the elastic Taylor–Couette instability in Boger fluids, Rheol. Acta 34 (2) (1995) 147–159.

[36] B.M. Baumert, S.J. Muller, Flow regimes in model viscoelastic fluids in a circular Couette system with independently rotating cylinders, Phys. Fluids 9 (3) (1997) 566–586.

[37] S.J. Muller, R.G. Larson, E.S. Shaqfeh, A purely elastic transition in Taylor–Couette flow, Rheol. Acta 28 (6) (1989) 499–503.

[38] S. Muller, E. Shaqfeh, R. Larson, Experimental studies of the onset of oscillatory instability in viscoelastic Taylor–Couette flow, J. Non-Newton. Fluid Mech. 46 (2–3) (1993) 315–330.

[39] R.G. Larson, E.S. Shaqfeh, S.J. Muller, A purely elastic instability in Taylor–Couette flow, J. Fluid Mech. 218 (1990) 573–600.

[40] E.S. Shaqfeh, S.J. Muller, R.G. Larson, The effects of gap width and dilute solution properties on the viscoelastic Taylor–Couette instability, J. Fluid Mech. 235 (1992) 285–317.

[41] Y.L. Joo, E.S. Shaqfeh, Observations of purely elastic instabilities in the Taylor–Dean flow of a Boger fluid, J. Fluid Mech. 262 (1994) 27–73.

[42] Y.L. Joo, E.S. Shaqfeh, A purely elastic instability in Dean and Taylor–Dean flow, Phys. Fluids A 4 (3) (1992) 524–543.

[43] Y.L. Joo, E.S. Shaqfeh, Viscoelastic Poiseuille flow through a curved channel: A new elastic instability, Phys. Fluids A 3 (9) (1991) 2043–2046.

[44] J. Zilz, R. Poole, M. Alves, D. Bartolo, B. Levaché, A. Lindner, Geometric scaling of a purely elastic flow instability in serpentine channels, J. Fluid Mech. 712 (2012) 203–218.

[45] J. Magda, R. Larson, A transition occurring in ideal elastic liquids during shear flow, J. Non-Newton. Fluid Mech. 30 (1) (1988) 1–19.

[46] G.H. McKinley, J.A. Byars, R.A. Brown, R.C. Armstrong, Observations on the elastic instability in cone-and-plate and parallel-plate flows of a polyisobutylene Boger fluid, J. Non-Newton. Fluid Mech. 40 (2) (1991) 201–229.

[47] J.A. Byars, A. Öztekin, R.A. Brown, G.H. Mckinley, Spiral instabilities in the flow of highly elastic fluids between rotating parallel disks, J. Fluid Mech. 271 (1994) 173–218.

[48] G.H. Mckinley, A. Öztekin, J.A. Byars, R.A. Brown, Self-similar spiral instabilities in elastic flows between a cone and a plate, J. Fluid Mech. 285 (1995) 123–164.

[49] R.G. Larson, Instabilities in viscoelastic flows, Rheol. Acta 31 (3) (1992) 213–263.

[50] R. Larson, S. Muller, E. Shaqfeh, The effect of fluid rheology on the elastic Taylor–Couette instability, J. Non-Newton. Fluid Mech. 51 (2) (1994) 195–225.

[51] A. Groisman, V. Steinberg, Couette–Taylor flow in a dilute polymer solution, Phys. Rev. Lett. 77 (8) (1996) 1480.

[52] A. Groisman, V. Steinberg, Solitary vortex pairs in viscoelastic Couette flow, Phys. Rev. Lett. 78 (8) (1997) 1460.

[53] A. Groisman, V. Steinberg, Elastic vs. inertial instability in a polymer solution flow, Europhys. Lett. 43 (2) (1998) 165.

[54] A. Groisman, V. Steinberg, Mechanism of elastic instability in Couette flow of polymer solutions: experiment, Phys. Fluids 10 (10) (1998) 2451–2463.

[55] V. Steinberg, A. Groisman, Elastic versus inertial instability in Couette–Taylor flow of a polymer solution, Phil. Mag. B 78 (2) (1998) 253–263.

[56] B.M. Baumert, S.J. Muller, Flow regimes in model viscoelastic fluids in a circular Couette system with independently rotating cylinders, Phys. Fluids 9 (3) (1997) 566–586.

[57] B.M. Baumert, S.J. Muller, Axisymmetric and non-axisymmetric elastic and inertio-elastic instabilities in Taylor–Couette flow, J. Non-Newton. Fluid Mech. 83 (1–2) (1999) 33–69.

[58] K.A. Kumar, M.D. Graham, Solitary coherent structures in viscoelastic shear flow: Computation and mechanism, Phys. Rev. Lett. 85 (19) (2000) 4056.

[59] K.A. Kumar, M. D. Graham, Finite-amplitude solitary states in viscoelastic shear flow: computation and mechanism, J. Fluid Mech. 443 (2001) 301.

[60] D. Thomas, U. Al-Mubaiyedh, R. Sureshkumar, B. Khomami, Time-dependent simulations of non-axisymmetric patterns in Taylor–Couette flow of dilute polymer solutions, J. Non-Newton. Fluid Mech. 138 (2–3) (2006) 111–133.

[61] D. Thomas, R. Sureshkumar, B. Khomami, Pattern formation in Taylor–Couette flow of dilute polymer solutions: dynamical simulations and mechanism, Phys. Rev. Lett. 97 (5) (2006) 054501.

[62] D. Thomas, B. Khomami, R. Sureshkumar, Nonlinear dynamics of viscoelastic Taylor–Couette flow: effect of elasticity on pattern selection, molecular conformation and drag, J. Fluid Mech. 620 (2009) 353.

[63] M. Avgousti, A.N. Beris, Viscoelastic Taylor–Couette flow: Bifurcation analysis in the presence of symmetries, Proc. R. Soc. Lond. Ser. A 443 (1917) (1993) 17–37.

[64] M. Renardy, Y. Renardy, R. Sureshkumar, A. Beris, Hopf-Hopf and steady-Hopf mode interactions in Taylor–Couette flow of an upper convected Maxwell liquid, J. Non-Newton. Fluid Mech. 63 (1) (1996) 1–31.

[65] H. Giesekus, Zur stabilität von strömungen viskoelastischer flüssigkeiten, Rheol. Acta 5 (3) (1966) 239–252.

[66] M. Avgousti, A.N. Beris, Non-axisymmetric modes in viscoelastic Taylor–Couette flow, J. Non-Newton. Fluid Mech. 50 (2–3) (1993) 225–251.

[67] S.J. Muller, Elastically-influenced instabilities in Taylor–Couette and other flows with curved streamlines: a review, Korea-Austr. Rheol. J. 20 (3) (2008) 117–125.

[68] L. Quinzani, G. McKinley, R. Brown, R. Armstrong, Modeling the rheology of polyisobutylene solutions, J. Rheol. 34 (5) (1990) 705–748.

[69] U. Al-Mubaiyedh, R. Sureshkumar, B. Khomami, Stability of viscoelastic Taylor–Couette flow: Influence of relaxation spectrum and energetics, in: 70th Annual Meeting of the Society of Rheology, Monterey, CA, 1998.

[70] U. Al-Mubaiyedh, R. Sureshkumar, B. Khomami, Linear stability of viscoelastic Taylor–Couette flow: influence of fluid rheology and energetics, J. Rheol. 44 (5) (2000) 1121–1138.

[71] P.J. Northey, R.C. Armstrong, R.A. Brown, Finite-amplitude time-periodic states in viscoelastic Taylor–Couette flow described by the UCM model, J. Non-Newton. Fluid Mech. 42 (1–2) (1992) 117–139.

[72] M.T. Arigo, L.E. Becker, G.H. McKinley, Viscous heating and non-isothermal hydrodynamics in polymer solutions, in: 70th Annual Meeting of the Society of Rheology, Monterey, CA, 1998.

[73] U. Al-Mubaiyedh, R. Sureshkumar, B. Khomami, Influence of energetics on the stability of viscoelastic Taylor–Couette flow, Phys. Fluids 11 (11) (1999) 3217–3226.

[74] M.J. Crochet, P.M. Naghdi, A class of simple solids with fading memory, Internat. J. Engrg. Sci. 7 (12) (1969) 1173–1198.

[75] U. Al-Mubaiyedh, R. Sureshkumar, B. Khomami, The effect of viscous heating on the stability of Taylor–Couette flow, J. Fluid Mech. 462 (2002) 111.

[76] J.M. White, S.J. Muller, Viscous heating and the stability of Newtonian and viscoelastic Taylor–Couette flows, Phys. Rev. Lett. 84 (2000) 5130–5133.

[77] J.M. White, S.J. Muller, Experimental studies on the stability of Newtonian Taylor–Couette flow in the presence of viscous heating, J. Fluid Mech. 462 (2002) 133–159.

[78] U. Al-Mubaiyedh, R. Sureshkumar, B. Khomami, Nonlinear stability analysis of viscoelastic Taylor–Couette flow in the presence of viscous heating, Phys. Fluids 14 (3) (2002) 1056–1064.

[79] Y.L. Joo, E.S. Shaqfeh, The effects of inertia on the viscoelastic Dean and Taylor–Couette flow instabilities with application to coating flows, Phys. Fluids A 4 (11) (1992) 2415–2431.

[80] D. Thomas, R. Sureshkumar, B. Khomami, Effect of inertia on thermoelastic flow instability, J. Non-Newton. Fluid Mech. 120 (1–3) (2004) 93–100.

[81] J.M. White, S.J. Muller, Experimental studies on the effect of viscous heating on the hydrodynamic stability of viscoelastic Taylor–Couette flow, J. Rheol. 47 (6) (2003) 1467–1492.

[82] A. Groisman, V. Steinberg, Elastic turbulence in curvilinear flows of polymer solutions, New J. Phys. 6 (1) (2004) 29.

[83] V. Steinberg, Elastic turbulence: An experimental view on inertialess random flow, Annu. Rev. Fluid Mech. 53 (2021) 27–58.

[84] S. Berti, A. Bistagnino, G. Boffetta, A. Celani, S. Musacchio, Two-dimensional elastic turbulence, Phys. Rev. E 77 (5) (2008) 055306.

[85] S. Berti, G. Boffetta, Elastic waves and transition to elastic turbulence in a two-dimensional viscoelastic Kolmogorov flow, Phys. Rev. E 82 (3) (2010) 036314.

[86] A. Groisman, V. Steinberg, Elastic turbulence in a polymer solution flow, Nature 405 (6782) (2000) 53–55.

[87] A. Groisman, V. Steinberg, Efficient mixing at low Reynolds numbers using polymer additives, Nature 410 (6831) (2001) 905–908.

[88] N. Liu, B. Khomami, Elastically induced turbulence in Taylor–Couette flow: direct numerical simulation and mechanistic insight, J. Fluid Mech. 737 (2013).

[89] I.M. Dris, E.S. Shaqfeh, On purely elsatic instabilities in eccentric cylinder flows, J. Non-Newton. Fluid Mech. 56 (3) (1995) 349–360.

[90] I. Dris, E.S. Shaqfeh, Flow of a viscoelastic fluid between eccentric cylinders: impact on flow stability, J. Non-Newton. Fluid Mech. 80 (1) (1998) 59–87.

[91] I.M. Dris, E.S. Shaqfeh, Experimental and theoretical observations of elastic instabilities in eccentric cylinder flows: local versus global instability, J. Non-Newton. Fluid Mech. 80 (1) (1998) 1–58.

[92] Y. Fan, R.I. Tanner, N. Phan-Thien, Fully developed viscous and viscoelastic flows in curved pipes, J. Fluid Mech. 440 (2001) 327–357.

[93] P. Pakdel, G.H. McKinley, Elastic instability and curved streamlines, Phys. Rev. Lett. 77 (12) (1996) 2459.

[94] U. Al-Mubaiyedh, R. Sureshkumar, B. Khomami, Energetic effects on the stability of viscoelastic Dean flow, J. Non-Newton. Fluid Mech. 95 (2–3) (2000) 277–293.

[95] K. Jackson, K. Walters, R. Williams, A rheometrical study of boger fluids, J. Non-Newton. Fluid Mech. 14 (1984) 173–188.

[96] T. Sridhar, An overview of the project M1, J. Non-Newton. Fluid Mech. 35 (2–3) (1990) 85–92.

[97] N. Phan-Thien, Cone-and-plate flow of the Oldroyd-B fluid is unstable, J. Non-Newton. Fluid Mech. 17 (1) (1985) 37–44.

[98] N. Phan-Thien, Coaxial-disk flow of an Oldroyd-B fluid: exact solution and stability, J. Non-Newton. Fluid Mech. 13 (3) (1983) 325–340.

[99] D.O. Olagunju, L.P. Cook, Secondary flows in cone and plate flow of an Oldroyd-B fluid, J. Non-Newton. Fluid Mech. 46 (1) (1993) 29–47.

[100] D.O. Olagunju, Elastic instabilities in cone-and-plate flow: small gap theory, Z. Angew. Math. Phys. 46 (6) (1995) 946–959.

[101] A. Öztekin, R.A. Brown, G.H. McKinley, Quantitative prediction of the viscoelastic instability in cone-and-plate flow of a Boger fluid using a multi-mode Giesekus model, J. Non-Newton. Fluid Mech. 54 (1994) 351–377.

[102] A. Öztekin, R.A. Brown, Instability of a viscoelastic fluid between rotating parallel disks: analysis of the Oldroyd-B fluid, J. Fluid Mech. 255 (1993) 473.

[103] A. Avagliano, N. Phan-Thien, Torsional flow stability of highly dilute polymer solutions, J. Non-Newton. Fluid Mech. 84 (1) (1999) 19–44.

[104] A. Avagliano, N. Phan-Thien, Torsional flow: elastic instability in a finite domain, J. Fluid Mech. 312 (1996) 279–298.

[105] Y. Renardy, M. Renardy, A model equation for axisymmetric stability of small-gap parallel-plate flows, J. Non-Newton. Fluid Mech. 77 (1–2) (1998) 103–114.

[106] D. Olagunju, On short wave elastic instabilities in parallel plate flow, ASME-PUBLICATIONS-FED 243 (1997) 243–248.

[107] J.P. Rothstein, G.H. McKinley, Non-isothermal modification of purely elastic flow instabilities in torsional flows of polymeric fluids, Phys. Fluids 13 (2) (2001) 382–396.

[108] D.O. Olagunju, Hopf bifurcation in creeping cone-and-plate flow of a viscoelastic fluid, Z. Angew. Math. Phys. 48 (3) (1997) 361–369.

[109] B.A. Toms, Some observations on the flow of linear polymer solutions through straight tubes at large Reynolds numbers, in: Proc. of in. Cong. on Rheology, 1948, vol. 135.

[110] J. Lumley, Drag reduction in turbulent flow by polymer additives, J. Polymer Sci. 7 (1973) 263–290.

[111] P. Virk, Drag reduction in rough pipes, J. Fluid Mech. 45 (2) (1971) 225–246.

[112] A. Roy, A. Morozov, W. van Saarloos, R.G. Larson, Mechanism of polymer drag reduction using a low-dimensional model, Phys. Rev. Lett. 97 (23) (2006) 234501.

[113] T. Min, J.Y. Yoo, H. Choi, D.D. Joseph, Drag reduction by polymer additives in a turbulent channel flow, J. Fluid Mech. 486 (2003) 213.

[114] N.S. Berman, Drag reduction of the highest molecular weight fractions of polyethylene oxide, Phys. Fluids 20 (5) (1977) 715–718.

[115] M. Tabor, P. De Gennes, A cascade theory of drag reduction, Europhys. Lett. 2 (7) (1986) 519.

[116] R. Sureshkumar, A.N. Beris, R.A. Handler, Direct numerical simulation of the turbulent channel flow of a polymer solution, Phys. Fluids 9 (3) (1997) 743–755.

[117] Y. Dubief, C.M. White, V.E. Terrapon, E.S. Shaqfeh, P. Moin, S.K. Lele, On the coherent drag-reducing and turbulence-enhancing behaviour of polymers in wall flows, J. Fluid Mech. 514 (2004) 271.

[118] C.-F. Li, R. Sureshkumar, B. Khomami, Influence of rheological parameters on polymer induced turbulent drag reduction, J. Non-Newton. Fluid Mech. 140 (1–3) (2006) 23–40.

[119] S. Belcher, N. Jerram, J. Hunt, Adjustment of a turbulent boundary layer to a'canopy'of roughness elements, J. Fluid Mech. 488 (2003) 369–398.

[120] G. Brethouwer, J. Hunt, F. Nieuwstadt, Micro structure and Lagrangian statistcs of the scalar field with a mean gradient in isotropic turbulence, J. Fluid Mech. 474 (2003) 193–225.

[121] M. Warholic, H. Massah, T. Hanratty, Influence of drag-reducing polymers on turbulence: effects of Reynolds number, concentration and mixing, Exp. Fluids 27 (5) (1999) 461–472.

[122] C.D. Dimitropoulos, R. Sureshkumar, A.N. Beris, Direct numerical simulation of viscoelastic turbulent channel flow exhibiting drag reduction: effect of the variation of rheological parameters, J. Non-Newton. Fluid Mech. 79 (2–3) (1998) 433–468.

[123] K.D. Housiadas, A.N. Beris, Polymer-induced drag reduction: Effects of the variations in elasticity and inertia in turbulent viscoelastic channel flow, Phys. Fluids 15 (8) (2003) 2369–2384.

[124] E. De Angelis, C. Casciola, R. Piva, DNS of wall turbulence: dilute polymers and self-sustaining mechanisms, Comput. & Fluids 31 (4–7) (2002) 495–507.

[125] C. Li, V. Gupta, R. Sureshkumar, B. Khomami, Turbulent channel flow of dilute polymeric solutions: drag reduction scaling and an eddy viscosity model, J. Non-Newton. Fluid Mech. 139 (3) (2006) 177–189.

[126] P. Ptasinski, B. Boersma, F. Nieuwstadt, M. Hulsen, B. Van den Brule, J. Hunt, Turbulent channel flow near maximum drag reduction: simulations, experiments and mechanisms, J. Fluid Mech. 490 (2003) 251.

[127] T. Min, H. Choi, J.Y. Yoo, Maximum drag reduction in a turbulent channel flow by polymer additives, J. Fluid Mech. 492 (2003) 91.

[128] R. Benzi, E. De Angelis, V.S. L'vov, I. Procaccia, Identification and calculation of the universal asymptote for drag reduction by polymers in wall bounded turbulence, Phys. Rev. Lett. 95 (19) (2005) 194502.

[129] L. Xi, M.D. Graham, Active and hibernating turbulence in minimal channel flow of Newtonian and polymeric fluids, Phys. Rev. Lett. 104 (21) (2010) 218301.

[130] K.R. Sreenivasan, C.M. White, The onset of drag reduction by dilute polymer additives, and the maximum drag reduction asymptote, J. Fluid Mech. 409 (2000) 149–164.

[131] C.-F. Li, R. Sureshkumar, B. Khomami, Simple framework for understanding the universality of the maximum drag reduction asymptote in turbulent flow of polymer solutions, Phys. Rev. E 92 (4) (2015) 043014.

[132] B.R. Elbing, M. Perlin, D.R. Dowling, S.L. Ceccio, Modification of the mean near-wall velocity profile of a high-Reynolds number turbulent boundary layer with the injection of drag-reducing polymer solutions, Phys. Fluids 25 (8) (2013) 085103.

[133] C. White, Y. Dubief, J. Klewicki, Re-examining the logarithmic dependence of the mean velocity distribution in polymer drag reduced wall-bounded flow, Phys. Fluids 24 (2) (2012) 021701.

[134] D. Samanta, Y. Dubief, M. Holzner, C. Schäfer, A.N. Morozov, C. Wagner, B. Hof, Elasto-inertial turbulence, Proc. Natl. Acad. Sci. 110 (26) (2013) 10557–10562.

[135] Y. Dubief, V.E. Terrapon, J. Soria, On the mechanism of elasto-inertial turbulence, Phys. Fluids 25 (11) (2013) 110817.

[136] S. Sid, V. Terrapon, Y. Dubief, Two-dimensional dynamics of elasto-inertial turbulence and its role in polymer drag reduction, Phys. Rev. Fluids 3 (1) (2018) 011301.

[137] G.H. Choueiri, J.M. Lopez, B. Hof, Exceeding the asymptotic limit of polymer drag reduction, Phys. Rev. Lett. 120 (12) (2018) 124501.

[138] J.M. Lopez, G.H. Choueiri, B. Hof, Dynamics of viscoelastic pipe flow at low Reynolds numbers in the maximum drag reduction limit, J. Fluid Mech. 874 (2019) 699–719.

[139] A. Shekar, R.M. McMullen, S.-N. Wang, B.J. McKeon, M.D. Graham, Critical-layer structures and mechanisms in elastoinertial turbulence, Phys. Rev. Lett. 122 (12) (2019) 124503.

[140] A. Shekar, R.M. McMullen, B.J. McKeon, M.D. Graham, Self-sustained elastoinertial Tollmien–Schlichting waves, J. Fluid Mech. 897 (2020).

[141] A. Fouxon, V. Lebedev, Spectra of turbulence in dilute polymer solutions, Phys. Fluids 15 (7) (2003) 2060–2072.

[142] V. Steinberg, Scaling relations in elastic turbulence, Phys. Rev. Lett. 123 (23) (2019) 234501.

[143] R. van Buel, C. Schaaf, H. Stark, Elastic turbulence in two-dimensional Taylor–Couette flows, Europhys. Lett. 124 (1) (2018) 14001.

[144] N. Liu, B. Khomami, Polymer-induced drag enhancement in turbulent Taylor–Couette flows: direct numerical simulations and mechanistic insight, Phys. Rev. Lett. 111 (11) (2013) 114501.

[145] J.-J. Lee, C.C. Mei, Stationary waves on an inclined sheet of viscous fluid at high Reynolds and moderate Weber numbers, J. Fluid Mech. 307 (1996) 191–229.

[146] N. Latrache, O. Crumeyrolle, I. Mutabazi, Transition to turbulence in a flow of a shear-thinning viscoelastic solution in a Taylor–Couette cell, Phys. Rev. E 86 (5) (2012) 056305.

[147] J. Song, H. Teng, N. Liu, H. Ding, X.-Y. Lu, B. Khomami, The correspondence between drag enhancement and vortical structures in turbulent Taylor–Couette flows with polymer additives: a study of curvature dependence, J. Fluid Mech. 881 (2019) 602–616.

[148] Y. Zhu, J. Song, N. Liu, X. Lu, B. Khomami, Polymer-induced flow relaminarization and drag enhancement in spanwise-rotating plane Couette flow, J. Fluid Mech. 905 (2020) A19.

[149] H. Teng, N. Liu, X. Lu, B. Khomami, Turbulent drag reduction in plane Couette flow with polymer additives: a direct numerical simulation study, J. Fluid Mech. 846 (2018) 482.

[150] J. Song, F. Lin, N. Liu, X.-Y. Lu, B. Khomami, Direct numerical simulation of inertio-elastic turbulent Taylor–Couette flow, J. Fluid Mech. 926 (2021) A37,1–29.

[151] J. Song, Z.-H. Wan, N. Liu, X.-Y. Lu, B. Khomami, A reverse transition route from inertial to elasticity-dominated turbulence in viscoelastic Taylor–Couette flow, J. Fluid Mech. 927 (2021) A10,1–12.

[152] M. Khalid, V. Shankar, G. Subramanian, A continuous pathway between the elasto-inertial and elastic turbulent states in viscoelastic channel flow, 2021, arXiv preprint arXiv:2103.06794.

[153] J. Rallison, E. Hinch, Do we understand the physics in the constitutive equation? J. Non-Newton. Fluid Mech. 29 (1988) 37–55.

[154] M. Chilcott, J.M. Rallison, Creeping flow of dilute polymer solutions past cylinders and spheres, J. Non-Newton. Fluid Mech. 29 (1988) 381–432.

[155] M. Bajaj, M. Pasquali, J.R. Prakash, Coil-stretch transition and the breakdown of computations for viscoelastic fluid flow around a confined cylinder, J. Rheol. 52 (1) (2008) 197–223.

[156] A. Abedijaberi, B. Khomami, Sedimentation of a sphere in a viscoelastic fluid: a multiscale simulation approach, J. Fluid Mech. 694 (2012) 78.

[157] K.D. Housiadas, J.P. Binagia, E.S. Shaqfeh, Squirmers with swirl at low Weissenberg number, J. Fluid Mech. 911 (2021).

[158] B. Yang, B. Khomami, Simulations of sedimentation of a sphere in a viscoelastic fluid using molecular based constitutive models, J. Non-Newton. Fluid Mech. 82 (2–3) (1999) 429–452.

[159] M. Yang, E.S. Shaqfeh, Mechanism of shear thickening in suspensions of rigid spheres in Boger fluids. Part I: Dilute suspensions, J. Rheol. 62 (6) (2018) 1363–1377.

[160] J. Hinch, A perspective of Batchelor's research in micro-hydrodynamics, J. Fluid Mech. 663 (2010) 8.

[161] W.R. Hwang, M.A. Hulsen, H.E. Meijer, Direct simulations of particle suspensions in a viscoelastic fluid in sliding bi-periodic frames, J. Non-Newton. Fluid Mech. 121 (1) (2004) 15–33.

[162] G. D'Avino, M.A. Hulsen, F. Snijkers, J. Vermant, F. Greco, P.L. Maffettone, Rotation of a sphere in a viscoelastic liquid subjected to shear flow. Part I: Simulation results, J. Rheol. 52 (6) (2008) 1331–1346.

[163] M. Yang, S. Krishnan, E.S. Shaqfeh, Numerical simulations of the rheology of suspensions of rigid spheres at low volume fraction in a viscoelastic fluid under shear, J. Non-Newton. Fluid Mech. 233 (2016) 181–197, http://dx.doi.org/10.1016/j.jnnfm.2016.05.004, URL https://www.sciencedirect.com/science/article/pii/S0377025716300593.

[164] J. Einarsson, M. Yang, E.S. Shaqfeh, Einstein viscosity with fluid elasticity, Phys. Rev. Fluids 3 (1) (2018) 013301.

[165] D.L. Koch, E.F. Lee, I. Mustafa, Stress in a dilute suspension of spheres in a dilute polymer solution subject to simple shear flow at finite Deborah numbers, Phys. Rev. Fluids 1 (1) (2016) 013301.

[166] R.I. Tanner, Rheology of noncolloidal suspensions with non-Newtonian matrices, J. Rheol. 63 (4) (2019) 705–717.

[167] D.L. Koch, G. Subramanian, The stress in a dilute suspension of spheres suspended in a second-order fluid subject to a linear velocity field, J. Non-Newton. Fluid Mech. 138 (2–3) (2006) 87–97.

[168] J. Rallison, The stress in a dilute suspension of liquid spheres in a second-order fluid, J. Fluid Mech. 693 (2012) 500.

[169] M. Yang, E.S. Shaqfeh, Mechanism of shear thickening in suspensions of rigid spheres in Boger fluids. Part II: Suspensions at finite concentration, J. Rheol. 62 (6) (2018) 1379–1396.

[170] Y. Matsuoka, Y. Nakayama, T. Kajiwara, Prediction of shear thickening of particle suspensions in viscoelastic fluids by direct numerical simulation, J. Fluid Mech. 913 (2021).

[171] A. Vázquez-Quesada, P. Español, R.I. Tanner, M. Ellero, Shear thickening of a non-colloidal suspension with a viscoelastic matrix, J. Fluid Mech. 880 (2019) 1070–1094.

[172] N. Jaensson, M. Hulsen, P. Anderson, Direct numerical simulation of particle alignment in viscoelastic fluids, J. Non-Newton. Fluid Mech. 235 (2016) 125–142.

[173] A. Jain, J. Einarsson, E.S. Shaqfeh, Extensional rheology of a dilute particle-laden viscoelastic solution, Phys. Rev. Fluids 4 (9) (2019) 091301.

[174] G. D'Avino, F. Greco, P.L. Maffettone, Particle migration due to viscoelasticity of the suspending liquid and its relevance in microfluidic devices, Annu. Rev. Fluid Mech. 49 (2017) 341–360.

[175] G. Li, G.H. McKinley, A.M. Ardekani, Dynamics of particle migration in channel flow of viscoelastic fluids, J. Fluid Mech. 785 (2015) 486–505.

[176] A.M. Leshansky, A. Bransky, N. Korin, U. Dinnar, Tunable nonlinear viscoelastic "focusing" in a microfluidic device, Phys. Rev. Lett. 98 (23) (2007) 234501.

[177] E. Carew, P. Townsend, M. Webster, A Taylor–Petrov–Galerkin algorithm for viscoelastic flow, J. Non-Newton. Fluid Mech. 50 (2–3) (1993) 253–287.

[178] M. Villone, G. D'Avino, M. Hulsen, F. Greco, P. Maffettone, Simulations of viscoelasticity-induced focusing of particles in pressure-driven micro-slit flow, J. Non-Newton. Fluid Mech. 166 (23–24) (2011) 1396–1405.

[179] G. d'Avino, P. Maffettone, F. Greco, M. Hulsen, Viscoelasticity-induced migration of a rigid sphere in confined shear flow, J. Non-Newton. Fluid Mech. 165 (9–10) (2010) 466–474.

[180] G. Gheissary, B. Van Den Brule, Unexpected phenomena observed in particle settling in non-Newtonian media, J. Non-Newton. Fluid Mech. 67 (1996) 1–18.

[181] K.D. Housiadas, R.I. Tanner, The drag of a freely sedimentating sphere in a sheared weakly viscoelastic fluid, J. Non-Newton. Fluid Mech. 183 (2012) 52–56.

[182] A. Zhang, W.L. Murch, J. Einarsson, E.S. Shaqfeh, Lift and drag force on a spherical particle in a viscoelastic shear flow, J. Non-Newton. Fluid Mech. 280 (2020) 104279.

[183] J. Einarsson, B. Mehlig, Spherical particle sedimenting in weakly viscoelastic shear flow, Phys. Rev. Fluids 2 (6) (2017) 063301.

[184] A. Zhang, W.L. Murch, J. Einarsson, E.S. Shaqfeh, Lift and drag force on a spherical particle in a viscoelastic shear flow, J. Non-Newton. Fluid Mech. 280 (2020) 104279, http://dx.doi.org/10.1016/j.jnnfm.2020.104279, URL https://www.sciencedirect.com/science/article/pii/S0377025720300471.

[185] W.L. Murch, S. Krishnan, E.S. Shaqfeh, G. Iaccarino, Growth of viscoelastic wings and the reduction of particle mobility in a viscoelastic shear flow, Phys. Rev. Fluids 2 (10) (2017) 103302.

[186] S. Krishnan, E.S. Shaqfeh, G. Iaccarino, Fully resolved viscoelastic particulate simulations using unstructured grids, J. Comput. Phys. 338 (2017) 313–338.

[187] C. Fernandes, S. Faroughi, O. Carneiro, J.M. Nóbrega, G. McKinley, Fully-resolved simulations of particle-laden viscoelastic fluids using an immersed boundary method, J. Non-Newton. Fluid Mech. 266 (2019) 80–94.

[188] S. Padhy, M. Rodriguez, E. Shaqfeh, G. Iaccarino, J. Morris, N. Tonmukayakul, The effect of shear thinning and walls on the sedimentation of a sphere in an elastic fluid under orthogonal shear, J. Non-Newton. Fluid Mech. 201 (2013) 120–129.

[189] S. Padhy, E. Shaqfeh, G. Iaccarino, J. Morris, N. Tonmukayakul, Simulations of a sphere sedimenting in a viscoelastic fluid with cross shear flow, J. Non-Newton. Fluid Mech. 197 (2013) 48–60.

[190] W.L. Murch, E.S. Shaqfeh, Collective effects in the sedimentation of particles in a viscoelastic fluid, Phys. Rev. Fluids 5 (7) (2020) 073301.

[191] D. Li, X. Xuan, Electrophoretic slip-tuned particle migration in microchannel viscoelastic fluid flows, Phys. Rev. Fluids 3 (7) (2018) 074202.

[192] A. Choudhary, D. Li, T. Renganathan, X. Xuan, S. Pushpavanam, Electrokinetically enhanced cross-stream particle migration in viscoelastic flows, J. Fluid Mech. 898 (2020).

[193] A.S. Khair, J.K. Kabarowski, Migration of an electrophoretic particle in a weakly inertial or viscoelastic shear flow, Phys. Rev. Fluids 5 (3) (2020) 033702.

[194] E. Allen, P. Uhlherr, Nonhomogeneous sedimentation in viscoelastic fluids, J. Rheol. 33 (4) (1989) 627–638.

[195] S. Bobroff, R.J. Phillips, Nuclear magnetic resonance imaging investigation of sedimentation of concentrated suspensions in non-Newtonian fluids, J. Rheol. 42 (6) (1998) 1419–1436.

[196] R. Vishnampet, D. Saintillan, Concentration instability of sedimenting spheres in a second-order fluid, Phys. Fluids 24 (7) (2012) 073302.

[197] G. Tiefenbruck, L. Leal, A numerical study of the motion of a viscoelastic fluid past rigid spheres and spherical bubbles, J. Non-Newton. Fluid Mech. 10 (1–2) (1982) 115–155.

[198] G. Tiefenbruck, L. Leal, A note on the slow motion of a bubble in a viscoelastic liquid, J. Non-Newton. Fluid Mech. 7 (2–3) (1980) 257–264.

[199] R. Zenit, J. Feng, Hydrodynamic interactions among bubbles, drops, and particles in non-Newtonian liquids, Annu. Rev. Fluid Mech. 50 (2018).

[200] J.R. Vélez-Cordero, D. Sámano, R. Zenit, Study of the properties of bubbly flows in Boger-type fluids, J. Non-Newton. Fluid Mech. 175 (2012) 1–9.